AIMS Biophysics

AIMS Biophysics, 13(3): 328−367.
DOI: 10.3934/biophy.2026019
Received: 30 June 2026
Revised: 22 August 2026
Accepted: 01 September 2026
Published: 09 September 2026

http://www.aimspress.com/journal/biophysics

Research article

A mathematical model of the glucocorticoid effects following preventive administration in a model of neuroinflammation

Elena Lebedeva[1,*], Ekaterina Kukushkina[1,2] and Marina Karpenko[1,2]

[1] Peter the Great St. Petersburg Polytechnic University, Saint Petersburg, Russia
[2] Laboratory of Neurochemistry, Pavlov Department of Physiology, Institute of Experimental Medicine, St. Petersburg, 197022, Russia

* **Correspondence:** Email: lebedeva.eya@edu.spbstu.ru; Tel: +79214167059.

Abstract: A mathematical model of neuroinflammation is proposed that describes the interplay among the peripheral inflammatory response, microglial activation, neural tissue damage, changes in blood–brain barrier permeability, and the effects of preventive glucocorticoid administration. The model is formulated as a system of ordinary differential equations and is intended to investigate the conditions governing the transition from an acute inflammatory response to a stable chronic state. The analysis includes verification of the models' well-posedness, identification of equilibria, local stability analysis, bifurcation analysis, and parameter sensitivity analysis. Three dynamic regimes were identified: rapid resolution of inflammation, delayed recovery accompanied by persistent changes in the central nervous system, and transition to chronic neuroinflammation. The development of chronic neuroinflammation was shown to be associated with strengthening of the positive feedback circuit between central inflammatory mediators and activated microglia. The parameters exerting the greatest influence on the duration of the inflammatory response, accumulation of neural tissue damage, and decline in the effectiveness of glucocorticoid-mediated regulation were identified. The model may be used to interpret experimental data, assess the contributions of individual components of the inflammatory response, and investigate the conditions underlying the development of chronic neuroinflammation.

Keywords: mathematical modeling; ordinary differential equations; neuroinflammation; glucocorticoids; bifurcation analysis

1. Introduction

Neuroinflammation is a complex immune response of the central nervous system (CNS) that develops in association with infectious, traumatic, and neurodegenerative processes. Its principal components include the activation of microglia and astrocytes, the release of pro-inflammatory cytokines, dysregulation of the blood–brain barrier (BBB), and neuronal damage. Neuroinflammation is currently regarded not merely as a secondary response to injury but also as an independent pathogenic mechanism capable of sustaining disease progression in Alzheimer's disease, Parkinson's disease, multiple sclerosis, and other CNS disorders [1,2].

Glucocorticoids (GCs) are C21 steroids that act mainly through the cytosolic glucocorticoid receptor (GR, NR3C1). Ligand binding dissociates the receptor from its chaperone complex and permits nuclear translocation, binding to glucocorticoid response elements and transactivation of anti-inflammatory genes, together with tethering-dependent transrepression of the pro-inflammatory transcription factors NF-κB and AP-1; the net effect is reduced transcription of IL-1β, TNF-α, IL-6, COX-2, and iNOS [3]. At intermediate and high concentrations, additional non-genomic mechanisms become quantitatively relevant: signaling through membrane-associated GR and nonspecific intercalation of the steroid into plasma and mitochondrial membranes, which alters cation transport and cellular bioenergetics within minutes and is not accompanied by changes in gene expression [4]. Because these two classes of mechanism have different concentration thresholds and different characteristic times, the pharmacological behavior of a given GC cannot be reduced to a single "anti-inflammatory potency" value.

Individual corticosteroids differ not in the nature of these mechanisms but in the structural features that determine receptor affinity, mineralocorticoid cross-reactivity, protein binding, and disposition. Introduction of a C1–C2 double bond into cortisol yields prednisolone (relative anti-inflammatory potency ≈ 4); 6α-methylation of prednisolone yields methylprednisolone (potency ≈ 5, duration of action 12–36 h); and 9α-fluorination combined with 16α-methylation yields dexamethasone (potency ≈ 30, no mineralocorticoid activity, duration of action 36–54 h) [5]. Dexamethasone and methylprednisolone are not the most potent corticosteroids in absolute terms: the relative receptor affinity of budesonide and mometasone furoate exceeds that of dexamethasone by approximately one and two orders of magnitude [6]. Affinity, however, is a measure of potency and not of efficacy, and in vitro rankings cannot be transferred directly to in vivo comparisons [7].

The criterion relevant here is therefore systemic and cerebral availability rather than maximal affinity. Budesonide and mometasone furoate were developed as topically acting agents, their high lipophilicity being deliberately combined with extensive first-pass metabolism and very low oral bioavailability, so that systemic—and hence cerebral—exposure is minimal by design [8]; they are unsuitable as a systemic intervention in endotoxemia. Prednisolone binds to corticosteroid-binding globulin to a saturable extent, so that its free fraction and clearance vary with dose, whereas dexamethasone and methylprednisolone are bound mainly to albumin and display dose-independent clearance, which makes their pharmacokinetics substantially easier to describe quantitatively [5]. Methylprednisolone additionally shows the highest non-genomic potency among the systemically used GCs, whereas dexamethasone combines the longest duration of action with the complete absence of mineralocorticoid activity [4,5,9]. These pharmacological arguments explain why the two agents were selected for the experimental protocol underlying the present model.

Delivery of GCs to brain tissue is nevertheless limited and compound-specific. Dexamethasone

is a substrate of the ABCB1 (P-glycoprotein) efflux transporter of the blood–brain barrier: in mdr1a-deficient mice, its cerebral uptake increases several-fold relative to wild-type animals, whereas its concentration in the pituitary, which lies outside the barrier, remains unchanged [10]. Cortisol and prednisolone are transported in a similar manner, while corticosterone is largely unaffected [11]. This restriction is not undisputed: in situ brain perfusion studies that controlled for capillary contamination and for the stability of the labeled compound reported a smaller and more heterogeneous contribution of P-glycoprotein, and results obtained in single- and double-knockout strains are not directly comparable [12]. What is not in dispute is that the cerebral concentration of a systemically administered GC is not proportional to its plasma concentration. Any quantitative description of GC action on neuroinflammation must therefore treat delivery to the brain as a separate, rate-limited process rather than as an instantaneous consequence of dosing.

Finally, the sign of the cerebral GC effect is not fixed. In addition to their canonical anti-inflammatory action in the CNS [13], GCs can act permissively and potentiate neuroinflammation. Prior exposure to GCs sensitizes ("primes") microglia: corticosterone administered 2 or 24 h before a peripheral LPS challenge potentiates the hepatic and hippocampal pro-inflammatory response, as well as the ex vivo response of isolated hippocampal microglia, whereas the same steroid given 1 h after the challenge suppresses it [14]. This priming has been attributed to GC-induced release of the alarmin HMGB1 and up-regulation of the NLRP3 inflammasome, which lowers the activation threshold of microglia for a subsequent stimulus [15]. The direction and the magnitude of the GC effect thus depend on dose, duration of exposure, the functional state of GR signaling, and—critically for preventive administration—on the timing of dosing relative to the inflammatory stimulus.

The experimental model of lipopolysaccharide (LPS)-induced endotoxemia is widely used to investigate systemic inflammation involving the CNS. This model makes it possible to examine the relationship between the peripheral inflammatory response, transmission of inflammatory signals to the brain, microglial activation, and neural tissue damage. However, interpretation of experimental data remains challenging because neuroinflammation is an inherently nonlinear process: the same inflammatory stimulus may result in rapid attenuation of the response, delayed resolution, progression to chronic inflammation, or a threshold-dependent transition to a stable pathological state.

Mathematical models formulated as systems of ordinary differential equations (ODEs) are increasingly used to describe such processes, as they enable quantitative analysis of the interactions among cytokines, immune cells, tissue damage, and pharmacological interventions [16,17]. Nevertheless, existing models often focus on individual components of the inflammatory cascade, provide only a limited representation of the interplay between peripheral and central inflammation, and do not adequately capture threshold-dependent dynamics. Consequently, they cannot fully explain why, under different parameter conditions, the system may evolve either toward resolution of inflammation or toward its chronic persistence.

Three specific gaps follow from the literature. First, published ODE models represent either the central cytokine–microglia–damage cascade [18,19] or the systemic inflammatory response, but rarely both compartments together with the barrier that couples them; transmission of the inflammatory signal from the periphery to the brain is consequently treated as a fixed gain rather than as a separate, state-dependent process. Second, where anti-inflammatory intervention has been modeled at all, it has been introduced as a direct reduction of a cytokine term or as an abstract control variable [20], without drug pharmacokinetics, without transfer across the blood–brain barrier, and without any representation of the time-dependent decline in GR-mediated efficacy; such formulations cannot reproduce the

experimentally documented dissociation between effective suppression of peripheral inflammation and persistent central inflammation. Third, no published model formalizes the dependence of the glucocorticoid effect on the timing of administration relative to the stimulus, although this dependence is the central experimental finding for preventive dosing [14]. Simply increasing model dimensionality is not a solution in itself, since immune models are difficult to identify from sparse time-course data [21], and spatial or multiscale formulations gain biological realism at the cost of analytical tractability [22].

In the present study, we propose a mathematical model of neuroinflammation that integrates the peripheral inflammatory component, central microglial activation, neural tissue damage, and the regulatory effects of glucocorticoids. Its novelty consists in addressing the three gaps identified above within a single system that remains amenable to analytical and numerical investigation. The model i) couples the peripheral and the central inflammatory compartments through an explicit and variable blood–brain barrier permeability, ii) represents glucocorticoid action as a chain of processes—plasma pharmacokinetics, restricted transfer into brain tissue, GR-mediated inhibition, and a time-dependent decline in the effectiveness of that inhibition—rather than as a fixed reduction of a cytokine term, and iii) makes the drug effect explicitly dependent on the interval between administration and the inflammatory stimulus, so that the preventive regimen used experimentally can be reproduced and analyzed. This formulation makes it possible to establish, by means of bifurcation and sensitivity analysis, the conditions under which preventive glucocorticoid administration attenuates neuroinflammation and those under which it fails to prevent the transition to a chronic state.

Unlike models that describe only the local dynamics of individual markers, the proposed approach treats neuroinflammation as an interconnected nonlinear system. It therefore enables analysis not only of temporal changes in the state variables but also of equilibrium stability, threshold-dependent transitions, parameter sensitivity, and the conditions underlying the establishment of a chronic inflammatory regime. The aim of this study was to develop a mathematical model of neuroinflammation that accounts for the preventive administration of glucocorticoids.

2. Materials and methods

2.1. Study design and protocol

The present work is a model-based (in silico) study. No new animal experiment was carried out; the study consists of the formulation, mathematical analysis, calibration, and numerical investigation of a deterministic model constructed on the basis of an experiment reported previously [23]. A deterministic system of ordinary differential equations was adopted as the modeling framework for three reasons. First, the available experimental readouts are group-mean values obtained at two time points, which does not support the identification of stochastic or spatially resolved formulations. Second, the question addressed here—whether preventive glucocorticoid administration prevents the transition to a chronic state or merely delays it—is a question about the qualitative organization of the phase space, and the equilibria of an ODE system, its stability, and its bifurcations can be examined both analytically and numerically. Third, a low-dimensional lumped formulation keeps the number of parameters commensurate with the amount of information contained in the data. Agent-based, spatially resolved, and multiscale formulations would provide greater biological detail but would be neither identifiable from the present data nor analytically tractable [21,22].

In order to make the procedure reproducible and to fix in advance the criteria by which the model would be judged, the study was carried out according to a fixed protocol, whose stages and conditions to be satisfied before proceeding to the next stage are summarized in Table 1.

Table 1. Study protocol: stages and conditions for proceeding.

Stage	Content of the stage	Result and condition for proceeding to the next stage
1	Definition of the biological scope from real-time PCR (IL-1β, TNF-α, iNOS, IBA-1) and histological readouts of the source experiment [23]	Every process represented corresponds to a measured or histologically assessed quantity
2	Formulation of the baseline system	Minimal system of four ODEs with nonlinear closure relations, amenable to analytical treatment
3	Stepwise extension of the system (B0 → A → B → C → final)	A version is retained only if the stated deficiency of its predecessor is removed without loss of analytical tractability (Table 2)
4	Parameterization and restricted calibration against the 12 group-mean values at 48 h and 10 days	Baseline parameter set within biologically plausible bounds and consistent with the experimental values (Subsection 2.4)
5	Qualitative analysis of the final system	Non-negativity and boundedness verified; equilibria located; local stability classified; bifurcations detected
6	Numerical experiments: control, LPS, GCs, GCs 2 h before LPS; LPS dose series 0.3, 1.0, and 5.0 mg/kg	Trajectories over 0–30 days (longer where persistence of the chronic state was examined); every integration converged
7	Sensitivity analysis (±5%, one-factor-at-a-time) and qualitative verification	Acceptance criteria (i)–(iv) satisfied, otherwise the model structure is revised

The formulation rests on the following assumptions, which are stated explicitly because they delimit the domain of validity of the results: (A1) The peripheral and the central inflammatory responses are each represented by a single lumped mediator variable rather than by individual cytokines; this is admissible because the expression of IL-1β, TNF-α, and iNOS changed concordantly in the experiment, and it is the reason why the model variables are dimensionless indices and not concentrations. (A2) Transfer of the inflammatory signal from the periphery to the brain is unidirectional and saturable, which reflects the limited capacity of the routes by which peripheral inflammation is signaled to the central nervous system. (A3) Microglial activation is a threshold-like and saturating process operating on a finite cell pool and is therefore described by a Hill function with an upper bound. (A4) Neural tissue damage is an aggregate variable that combines the morphological signs assessed histologically and is not equated with the loss of a defined number of neurons. (A5) Glucocorticoid disposition is described by a minimal two-compartment scheme comprising a central and an effect compartment; dexamethasone and methylprednisolone share this structure and differ in an exposure scaling factor, because drug-specific pharmacokinetic measurements were not available in the source experiment. (A6) The reduction in glucocorticoid receptor-mediated efficacy is driven by

cumulative drug exposure and by the inflammatory stimulus and relaxes with a first-order rate. (A7) Each experimental group is represented by a single average trajectory; inter-individual variability is not modeled.

The criteria for accepting the model were fixed before the numerical experiments were performed. The model was required to (1) generate no inflammatory response in the absence of lipopolysaccharide, and in particular not to permit glucocorticoid administration alone to initiate inflammation; (2) reproduce the ordering of the experimental groups at 48 h and at 10 days, that is, lipopolysaccharide > glucocorticoid + lipopolysaccharide > control for the central inflammatory and microglial indices; (3) reproduce the persistence of central alterations at 10 days despite resolution of the peripheral response; and (4) preserve non-negativity and boundedness of the solutions over the whole range of admissible parameter values. Failure of any of these criteria was treated as grounds for revising the structure of the model rather than for further adjustment of its parameters; the transitions between the model versions listed in Table 2 were made on precisely this basis.

2.2. Experimental basis of the mathematical model

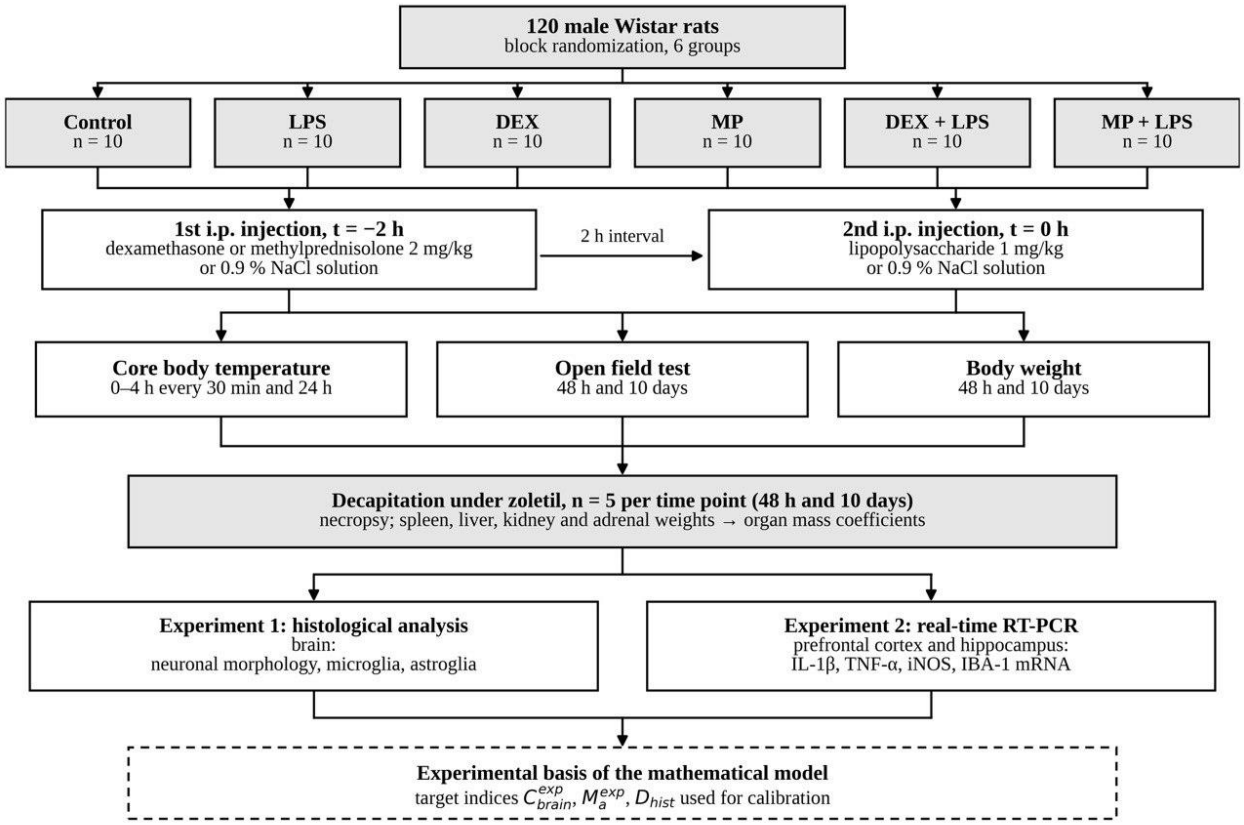

Figure 1. Overall design of the experimental study underlying the mathematical model of neuroinflammation under preventive administration of glucocorticoids. DEX, dexamethasone; MP, methylprednisolone; LPS, lipopolysaccharide; i.p., intraperitoneal; RT-PCR, real-time reverse transcription polymerase chain reaction; n, number of animals per group; t, time relative to LPS administration. The dashed box indicates the transition from the experimental readouts to the target indices used for model calibration.

The model builds on a previously published experimental investigation of glucocorticoid effects in rats with lipopolysaccharide-induced endotoxemia [23], performed on 120 male Wistar rats allocated by block randomization into six groups (n = 10 per group). The overall design—the administration protocol, the recorded measures, the observation time points, and the distribution of the biological material between the analytical blocks—is presented in Figure 1, and the measures were subsequently converted into the target integral indices used in the numerical calibration of the model (Subsection 3.8).

The animals received a single intraperitoneal injection of lipopolysaccharide at a dose of 1 mg/kg, dexamethasone at 2 mg/kg, methylprednisolone at 2 mg/kg, or the corresponding glucocorticoid 2 h before lipopolysaccharide; the control group received an equivalent volume of 0.9% sodium chloride solution. Changes were assessed 48 h and 10 days after administration of the inflammatory stimulus. Histological examination covered signs of microglial activation, acidophilic neuronal necrosis and chromatolysis, and changes in cellularity, and quantitative real-time PCR was used to determine the relative mRNA expression of IL-1β, TNF-α, iNOS, and IBA-1 in the prefrontal cortex and hippocampus.

The PCR and histological findings are not presented in the present article as an independent experimental dataset. Instead, they served as the biological basis for defining the mathematical model structure, selecting its principal variables, and specifying the relationships among the peripheral inflammatory response, central pro-inflammatory mediators, microglial activation, neural tissue damage, and glucocorticoid action. These findings were also considered when selecting the characteristic time scales of the model and interpreting the early and delayed dynamics of neuroinflammation.

The experimental procedures, the conditions under which the animals were housed, the composition and size of the experimental groups, and the ethical approval of the protocol are reported in full in the original publication [23]. The present study used only the summary values derived from that work and involved no additional experimental procedures on animals.

2.3. Development and structure of the mathematical model

The experimental observations described in the preceding subsection were used to formulate the biological concept of the model and to identify the principal processes that needed to be represented in the mathematical system.

General principle underlying the model equations: All equations of the model are constructed from a single principle, the local balance of an extensive quantity. For every state variable, the rate of change is written as the difference between production and elimination, $dX_i/dt = P_i(X) - E_i(X)$, with non-negative production and elimination functions. Equations (1), (2), (3), and (6) are particular cases of this relation applied to circulating lipopolysaccharide, to central inflammatory mediators, to the microglial pool, and to accumulated tissue damage. Three postulates fix its mathematical form and explain why the system consists of first-order ordinary differential equations. First, each compartment is treated as well mixed, so that no spatial gradients arise, and the model is a system of ordinary rather than partial differential equations. Second, the instantaneous rates depend only on the current state, so that no delay terms appear, and the finite time required for the response to develop is reproduced by the chain L → C → Ma → D rather than by explicit delays. Third, the cell and molecular populations are large, so that the description is deterministic, and the trajectories are to be interpreted as group

means.

Only three types of constitutive relations are used: (1) First-order removal: elimination of lipopolysaccharide, clearance of mediators, deactivation of microglia, and resolution of damage are written as rates proportional to the quantity present, the standard assumption for processes operating far from saturation. (2) Additive independent sources: in equation (2), the signal originating from circulating lipopolysaccharide and the secretion by activated microglia enter as a sum, since a multiplicative coupling would imply that neither source can act in the absence of the other, contrary to the persistence of central changes after lipopolysaccharide has been cleared. (3) Saturating rate laws of the Hill type: receptor-mediated processes operate on a finite number of binding sites, so that the rate is a Hill function of the stimulus with a half-saturation constant and an exponent n, where n > 1 encodes the cooperativity responsible for the threshold-like response of microglia; the same argument applies to the contribution of tissue damage to the activation stimulus and to transfer across the blood–brain barrier. Equation (3) is a balance not of a substance but of cells between the resting and the activated states under a conserved total, which is why the activation rate is multiplied by the number of cells still available for recruitment. Every removal term contains its own variable as a factor, and this is the structural reason for the non-negativity and boundedness of the solutions established in Subsection 3.1. All coefficients have the dimension of the corresponding variable divided by time, with time being measured in days.

At the first stage, a basic system of ordinary differential equations was formulated to describe the dynamics of neuroinflammation following a single systemic administration of lipopolysaccharide (LPS): (1) the kinetics of circulating LPS, (2) the level of pro-inflammatory mediators in the brain, (3) the degree of microglial activation as a key effector of the innate immune response in the central nervous system, and (4) the extent of neuronal damage. The principal state variables governing neuroinflammation are defined as follows:

- L(t): effective circulating LPS level; L (0) = L_0, where L_0 denotes the administered LPS dose (mg/kg).
- C(t): level of pro-inflammatory cytokines and other mediators of neuroinflammation in the brain.
- Ma(t): degree of microglial activation, normalized to the interval $0 \leq Ma \leq Ma_{max}$.
- D(t): neuronal damage, representing morphological alterations in the CNS.

The blood concentration of LPS decreases as a result of its elimination from the circulation. Circulating LPS and activated microglia stimulate the production of pro-inflammatory mediators, which, in turn, sustain microglial activation and promote the accumulation of neuronal damage. Damaged neurons further enhance microglial activation, thereby establishing a positive feedback circuit. It is this self-reinforcing cytokine–microglia–damage loop that converts an initially protective reaction into a sustained inflammatory state in the central nervous system [24].

The blood concentration of LPS is described by a first-order elimination equation (1):

$$\frac{dL}{dt} = -\delta_L L,\ L(0) = D_{LPS} \tag{1}$$

The dynamics of pro-inflammatory mediators in the brain are determined by their production in response to LPS and activated microglia, together with their clearance (2):

$$\frac{dC}{dt} = \beta_C Ma + \sigma_L(L) - \delta_C^{eff}(D_{LPS})C \tag{2}$$

Microglial activation is described by a saturating Hill function (3):

$$\frac{\mathrm{dMa}}{\mathrm{dt}} = \kappa_{\mathrm{in}} \frac{\mathrm{stim}^{\mathrm{n}}}{\mathrm{K}^{\mathrm{n}}+\mathrm{stim}^{\mathrm{n}}} (\mathrm{Ma}_{\mathrm{max}} - \mathrm{Ma}) - \kappa_{\mathrm{out}} \mathrm{Ma} \quad (3)$$

The equation describes the transition of microglia to the activated state (4) in response to inflammatory stimuli, followed by their subsequent deactivation.

Activation term:

$$\kappa_{\mathrm{in}} \frac{\mathrm{stim}^{\mathrm{n}}}{\mathrm{K}^{\mathrm{n}}+\mathrm{stim}^{\mathrm{n}}} (\mathrm{Ma}_{\mathrm{max}} - \mathrm{Ma}) \quad (4)$$

The parameter κ_{in} defines the maximum activation rate. The Hill function $\frac{stim^n}{K^n+stim^n}$ captures the threshold-like and saturating nature of microglial activation: the response remains weak at low stimulus levels and approaches saturation as the stimulus increases. The parameter (K) denotes the half-saturation constant, or effective activation threshold, whereas (n) determines the degree of cooperativity and the steepness of the activation response. The factor $(Ma_{max} - Ma)$ imposes an upper bound, interpreted as the maximum attainable level of activation or the maximal fraction of cells capable of transitioning to the activated state.

Deactivation term: The term $-\kappa_{out}$ represents the rate at which microglia return to the basal phenotype in the absence of a sustained activating stimulus. Higher values of $-\kappa_{out}$ correspond to a more rapid decay of the microglial response.

The total stimulus driving microglial activation is defined as follows (5):

$$stim = \tilde{\delta} L + \eta^{eff}(D_{LPS}) C + \rho^{eff}(D_{LPS}) \frac{D}{K_D+D} \quad (5)$$

The stimulus comprises three components. The term $\tilde{\delta} L$ represents the direct effect of LPS on microglia and reflects innate immune activation in response to a systemic inflammatory stimulus. The term $\eta^{eff}\mathrm{C}$ represents the contribution of cytokines and establishes the positive feedback loop C→ Ma→ C. The term $\rho^{eff}(D_{LPS}) \frac{D}{K_D+D}$ describes the contribution of neuronal damage as a secondary driver of inflammation. The saturating function $\frac{D}{K_D+D}$ limits the effect of damage at high values of D, whereas KD denotes the corresponding half-saturation constant. Under the high-dose regime, the contribution of neuronal damage is enhanced, $\rho^{eff}(D_{LPS}) = \rho\big(1 + b_N N(D_{LPS})\big)$ according to the generation of a self-sustaining pathological feedback circuit: D→ Ma →C →D.

The accumulation of neuronal damage is described by equation (6):

$$\frac{dD}{dt} = k_{in}^{eff}(D_{LPS}) C - k_{out} D \quad (6)$$

This equation relates the accumulation of neuronal damage to the level of inflammatory mediators. The term $k_{in}^{eff} C$ represents the cytokine-to-damage relationship and integrates both the duration and the intensity of the inflammatory response. The effective rate of damage accumulation increases at LPS doses of 5 mg/kg or higher, corresponding to the high-dose regime: $k_{in}^{eff}(D_{LPS}) = k_{in}\big(1 + a_N N(D_{LPS})\big)$. This formulation makes it possible to describe the dose-dependent transition toward chronic neuroinflammation as the LPS dose increases. The term $-k_{out} D$ represents repair and compensatory processes or a reduction in the magnitude of the integral damage variable. At low values

of k_{out}, damage persists for an extended period, whereas higher values of k_{out} are associated with a more rapid resolution of neuroinflammation.

To describe the dependence of the inflammatory response pattern on the administered LPS dose, smoothed switching functions were introduced into the model (7). Here, L0 denotes the fixed initial dose administered at t = 0, whereas L(t) denotes the time-dependent residual LPS stimulus governed by the elimination equation. The regime-switching functions, therefore, depend on L0 rather than on L(t).

$$S_1(D_{LPS}) = \frac{D_{LPS}^p}{1^p + D_{LPS}^p},\ S_5(D_{LPS}) = \frac{D_{LPS}^p}{5^p + D_{LPS}^p}, \tag{7}$$

The parameter p determines the steepness of the transition. The first switching function is activated at an administered dose L0 of approximately 1 mg/kg, whereas the second is activated at approximately 5 mg/kg. The priming window is defined as follows (8):

$$P(D_{LPS}) = S_1(D_{LPS})\big(1 - S_5(D_{LPS})\big), \tag{8}$$

The dose-dependent function P(L0) takes values close to unity predominantly within the range $1.0 \leq L0 \leq 5.0$ mg/kg and approaches zero at both lower and higher administered doses. Biologically, this behavior is interpreted as a microglial priming regime in which inflammation becomes more persistent and prolonged owing to reduced efficiency of inflammatory resolution and increased microglial sensitivity.

The transition to chronic neuroinflammation is represented by the following function (9):

$$\mathrm{N}(\mathrm{D_{LPS}}) = \mathrm{S_5}(\mathrm{D_{LPS}}), \tag{9}$$

The dose-dependent function N(L0) becomes active when the administered dose L0 exceeds 5 mg/kg and enhances the damage-promoting and self-sustaining feedback mechanisms. At low doses (0.1–1.0 mg/kg), the system returns to its basal state through LPS elimination, mediator clearance, and microglial deactivation. At intermediate doses, P(L0) reduces mediator clearance and strengthens cytokine-microglia coupling. At high doses, N(L0) enhances damage accumulation and the feedback effect of tissue damage on microglia, thereby generating a self-sustaining pathological loop.

Effective cytokine clearance (10):

$$\delta_C^{eff}(D_{LPS}) = \frac{\delta_C}{1 + a_P P(D_{LPS})} \tag{10}$$

A decrease in δ_C^{eff} when P(L0) ≈ 1 prolongs the persistence of C(t) and promotes the transition toward a chronic inflammatory response.

Effective microglial sensitivity to cytokines (11)

$$\eta^{eff}(D_{LPS}) = \eta\big(1 + b_P P(D_{LPS})\big) \tag{11}$$

An increase in η^{eff} strengthens the positive feedback circuit C→ Ma→C, thereby reducing the likelihood of rapid resolution of the inflammatory response at intermediate LPS doses.

Effective rate of damage formation (12):

$$k_{in}^{eff}(D_{LPS}) = k_{in}(1 + a_N N(D_{LPS})) \tag{12}$$

An increase in k_{in}^{eff} under the high-dose regime causes the same cytokine level to produce a greater accumulation of neuronal damage D(t).

Effective contribution of damage to the microglial activation stimulus (13):

$$\rho^{eff}(D_{LPS}) = \rho(1 + b_N N(D_{LPS})) \tag{13}$$

An increase in ρ^{eff} when N (L0) ≈ 1 makes neuronal damage an independent driver of inflammation and enables self-sustained propagation of the inflammatory cascade after LPS has been eliminated. This behavior corresponds to the development of chronic neuroinflammation.

Thus, the resulting system of nonlinear ordinary differential equations describing the neuroinflammatory process can be written as follows:

$$\begin{cases} \frac{dL}{dt} = -\delta_L L, L(0) = D_{\text{LPS}}, \\ \frac{dC}{dt} = \beta_C Ma + \sigma_L(L) - \delta_C^{\text{eff}}(D_{\text{LPS}})C, \\ \frac{dMa}{dt} = \kappa_{in} \frac{\text{stim}^n}{K^n + \text{stim}^n}(Ma_{\max} - Ma) - \kappa_{out} Ma, \\ \frac{dD}{dt} = k_{in}^{\text{eff}}(D_{\text{LPS}})C - k_{out} D. \end{cases}$$

$$stim = \tilde{\delta} L + \eta^{eff}(D_{LPS})C + \rho^{eff}(D_{LPS})\frac{D}{K_D + D}.$$

$$C(0) = 0, \qquad Ma(0) = 0, \qquad D(0) = 0.$$

The model described above captures the dynamics of the principal components of the neuroinflammatory response following LPS administration, but it does not account for the pharmacokinetics of glucocorticoids, the distinction between peripheral and central inflammatory responses, or time-dependent changes in the effectiveness of glucocorticoid-mediated regulation. The system was therefore expanded in a stepwise manner, each step removing one specific deficiency of the preceding version. For every version, Table 2 states what was added, which state variables the system then contained, which experimental observation it became able to reproduce, and which limitation remained and therefore motivated the next step.

Table 2. Stepwise modification of the mathematical model: what each version adds, what it reproduces, and which limitation motivates the next step.

Step (version)	What is added relative to the preceding version	State variables	What the version becomes able to reproduce	Limitation that remains: reason for the next step
Baseline system	(starting point: LPS-induced neuroinflammation without treatment)	L, C, Ma, D	Acute response to LPS; microglial activation; accumulation of damage; dose-dependent regimes	Glucocorticoids are absent, so the treated experimental groups cannot be simulated
B0: Simplified model with GCs	A single glucocorticoid variable X(t) inhibiting the inflammatory term directly	L, C, Ma, D, X	Suppression of the response by GCs; preventive dosing enters only through $X(0) = X_{pre}$	The effect follows plasma exposure instantaneously, so the delay between dosing and response is not reproduced
A: Delayed GCs effect	An effect compartment separating plasma exposure from the exposure that drives the response	L, C, Ma, D, X_c, X_e	The lag between dosing and effect; the preventive regimen becomes a property of the dynamics rather than of the initial condition	A single inhibitory pathway, so the effect on mediator production cannot be distinguished from that on microglial activation
B: Two inhibitory pathways	Two inhibitory functions: I_C on mediator production and I_N on the activation stimulus	L, C, Ma, D, X_c, X_e	Different profiles of suppression of the mediator and the microglial components at the same dose	C remains aggregated and belongs to neither compartment; there is no explicit peripheral-to-brain coupling
C: Peripheral–central model with BBB coupling	Separation of the mediator variable into a peripheral and central pool linked by a saturable flux J_{BBB}	L, C_{per}, C_{brain}, Ma, D, X_c, X_e	Peripheral suppression together with a sustained central response; direct correspondence with the PCR and histological readouts	Inhibitory efficacy is constant in time; the pharmacokinetic block remains oversimplified

Continued on next page

Step (version)	What is added relative to the preceding version	State variables	What the version becomes able to reproduce	Limitation that remains: reason for the next step
Final: PK block and variable R(t)	One-compartment pharmacokinetics with an effect compartment (Eq. 14) and R(t) for the decline in GR-mediated efficacy (Eq. 15)	L, X_c, X_e, C_{per}, C_{brain}, Ma, D, R	All four experimental patterns: peripheral suppression, incomplete central suppression, persistence at day 10, and dependence on the timing of administration	Version adopted for analysis

Modification C removed the ambiguity of the aggregated mediator variable by separating it into a peripheral and a central pool, providing a substantially more rigorous basis for biological interpretation and for comparison with the experimental data. The final model additionally incorporates a minimal one-compartment pharmacokinetic block with an effect compartment (14), which accounts for the delay between systemic exposure and the pharmacodynamic response and thus reproduces the protocol in which glucocorticoids were given 2 h before the LPS challenge, and the variable R(t) (15), whose increase reduces the effectiveness of the inhibitory drug action and makes it possible to reproduce incomplete suppression of the central inflammatory response despite a simultaneous reduction in peripheral inflammation. The final system of ODEs is given by:

$$\begin{cases} \dfrac{dL}{dt} = -\delta_L L, \qquad L(0) = D_{\mathrm{LPS}} \\ \dfrac{dX_c}{dt} = -k_{el} X_c, \qquad \dfrac{dX_e}{dt} = k_{e0}(X_c - X_e) \quad (14) \\ \dfrac{dR}{dt} = k_{RX} \dfrac{X_e^q}{EC_{50,R}^q + X_e^q} + k_{RS} \dfrac{\mathrm{stim}_0^r}{K_R^r + \mathrm{stim}_0^r} - \delta_R R \quad (15) \\ \dfrac{dC_{\mathrm{per}}}{dt} = \sigma_L(L)\, I_C(X_e, R) - \delta_{\mathrm{per}}\, C_{\mathrm{per}}, \\ \dfrac{dC_{\mathrm{brain}}}{dt} = \beta_{\mathrm{brain}}\, Ma + J_{\mathrm{BBB}}(C_{\mathrm{per}}) - \delta_{\mathrm{brain}}^{\mathrm{eff}}(D_{\mathrm{LPS}})\, C_{\mathrm{brain}}, \\ \dfrac{dMa}{dt} = \kappa_{in} \dfrac{\mathrm{stim}^n}{K^n + \mathrm{stim}^n} (Ma_{\max} - Ma) - \kappa_{out} Ma \\ \dfrac{dD}{dt} = k_{in}^{\mathrm{eff}}(D_{\mathrm{LPS}})\, C_{\mathrm{brain}} - k_{out} D \end{cases}$$

Blood–brain barrier:

$$J_{BBB}(C_{per}) = k_{BBB} \frac{C_{per}}{K_{BBB} + C_{per}}.$$

Central inflammatory stimulus:

$$stim_0 = \tilde{\delta} L + \eta^{eff}(D_{LPS}) C_{brain} + \rho^{eff}(D_{LPS}) \frac{D}{K_D + D}.$$

$$stim = I_N(X_e, R) stim_0.$$

Glucocorticoid inhibitory functions:

$$I_C(X_e, R) = \frac{1}{1 + \left(\frac{X_e}{IC_{50,C}^{eff}(R)} \right)^{n_C}}, I_N(X_e, R) = \frac{1}{1 + \left(\frac{X_e}{IC_{50,N}^{eff}(R)} \right)^{n_N}}$$

$$IC_{50,C}^{eff}(R) = IC_{50,C}(1 + \alpha_C R), IC_{50,N}^{eff}(R) = IC_{50,N}(1 + \alpha_N R).$$

The dose-dependent effective coefficients δ_{brain}^{eff}, k_{in}^{eff}, η^{eff}, and ρ^{eff} and the smoothed dose-regime switching functions P_{dose} and N_{dose} retain the forms introduced in equations (7)–(13), with δ_{brain} in place of δ_C.

The selected structure is a minimal model of sufficient complexity: it is consistent with the experimental design and permits investigation of the differences between the peripheral and the central effects of glucocorticoids, of incomplete suppression of neuroinflammation, and of the persistence of a delayed inflammatory response, while integrating the principal components of the system within a unified dynamical framework. It does not encompass all molecular and cellular mechanisms of neuroinflammation, and further refinement would require additional variables and parameters that cannot be reliably identified from the available experimental data. The present formulation therefore preserves biological interpretability at the level of detail the data can support.

2.4. Parameter selection and model scaling

Parameterization of the final ODE model was performed with consideration of the experimental conditions, the biological meaning of the processes included, published data, and the results of mathematical analysis of the system.

For parameters governing nonlinear interactions and threshold effects, the results of equilibrium, stability, and bifurcation analyses were additionally taken into account. Particular attention was given to the parameters of the central positive feedback circuit, because changes in these parameters determined whether a stable chronic state and bistability could emerge. Thus, the final parameter values reflected not only biological considerations but also the requirements imposed by the dynamical behavior of the model.

Time was measured in days. Lipopolysaccharide and glucocorticoid doses were specified in mg/kg. Variables describing peripheral and central inflammatory mediators, blood–brain barrier status, microglial activation, neural tissue damage, and reduced efficiency of glucocorticoid receptor-mediated signaling were expressed as normalized dimensionless quantities. This scaling enabled the different components of the system to be compared within a unified mathematical framework without equating the integral model variables with the concentrations of individual cytokines or the expression levels of specific genes.

The baseline values listed in Table 3 come from five types of sources. Three parameters are fixed

by the experimental protocol (the glucocorticoid dose, the interval between drug and lipopolysaccharide, and the lipopolysaccharide dose). Eight rate constants are inverse characteristic times and were chosen so that the associated half-lives lie within the range known from the literature, from 6.2 h for the clearance of central mediators to 23.8 h for the recovery of GR-signaling efficiency; these quantities characterize the functional dynamics of the measured markers and not the clearance of molecules from plasma, since lipopolysaccharide is eliminated from the bloodstream within minutes, whereas the pro-inflammatory gene expression it induces persists for tens of hours. Seven parameters differ between the dynamic regimes (Table 7) and were chosen according to their position relative to the bifurcation threshold, and eight were determined by numerical calibration (Table 11); the dose-dependent potentiation coefficients a_P, a_N, b_P, and b_N are zero in the baseline set and are switched on only when dosing regimens are simulated.

Five parameters—Ma_{max}, K, K_D, K_{BBB}, and σ_{max}—constitute a normalization convention and cannot be determined from the data even in principle, because the system admits five independent one-parameter groups of transformations that leave all observable quantities unchanged: rescaling Ma_{max} and β_{brain} reciprocally, for example, multiplies Ma by the same factor while leaving C_{brain} and D unaltered, and is absorbed by the observation scaling factor s_M. Analogous groups exist for the scales of C_{brain}, C_{per}, and D and for the scale of the total stimulus together with K; numerical verification confirms the invariance to within 10^{-10} to 10^{-16}. The values of these five parameters were therefore chosen so that the model variables take values of order unity; they were excluded from calibration.

The nonlinearity exponents were chosen on mechanistic rather than statistical grounds: for a Hill exponent $n = 1$ in the microglial activation function, bistability is absent, whereas for any $n > 1$, the system has three equilibria and the physiological state is stable, so that cooperativity of activation is a structural requirement of the model; the particular value $n = 4$ affects only the steepness of the transition. The evenness of the exponents additionally ensures smoothness of the right-hand side near the boundary of the non-negative orthant, which is used in the proof of well-posedness. The two remaining shape constants, D_{crit} and $EC50_R$, were adopted without direct justification; under random variation of both within ±50%, the structure of the dynamic regimes was preserved in all 60 runs, and the ranking of the parameters by sensitivity was unchanged.

So that the baseline parameter set should not rest on manual adjustment alone, a restricted numerical calibration of the third group of parameters was performed against the group-mean experimental values at 48 h and at 10 days in the prefrontal cortex and in the hippocampus for the three experimental groups; that is, 12 observation points. The procedure, objective function, and its weights are described in Subsections 3.9 and 3.10. With 12 observation points and only 2 sampling times, this is a restricted calibration of a subset of coefficients rather than a complete independent identification of the model: it places the baseline parameter set within a biologically admissible region consistent with the experimental values and does not by itself establish structural identifiability.

The baseline parameter values of the final model, their biological interpretation, units of measurement, and methods of determination are presented in Table 3.

Table 3. Baseline parameter values of the final mathematical model.

Parameter	Biological meaning	Baseline value
δ_L	LPS clearance rate	1.20
δ_{per}	Peripheral cytokine clearance rate	1.00
δ_{brain}	Central inflammatory mediator clearance rate	2.677
k_{BBB}	Peripheral-to-brain transport/signaling across the BBB	0.30
K_{BBB}	Half-saturation constant of BBB-mediated signaling	0.50
β_{brain}	Production of central inflammatory mediators by activated microglia	1.538
η	Microglial sensitivity to central inflammatory mediators	2.863
ρ	Contribution of tissue damage to microglial activation	2.103
k_{in}	Damage accumulation rate	0.370
k_{out}	Tissue repair/damage resolution rate	1.224
κ_{in}	Microglial activation rate	2.258
κ_{out}	Microglial deactivation rate	1.179
Ma_{max}	Maximum microglial activation level	1.570
K	Microglial activation threshold	1.164
n	Hill coefficient	4
X_{dose}	GCs dose	2 mg/kg
k_{el}	Elimination rate from the central PK compartment	1.8
k_{e0}	Exchange rate between the central and effect compartments	1.4
IC50,C	Half-maximal concentration for peripheral inhibition	0.8
IC50,N	Half-maximal concentration for central inhibition	0.8
α_C	Increase in IC50,C associated with reduced GR sensitivity	0.5
α_N	Increase in IC50,N associated with reduced GR sensitivity	0.5
k_{RX}	Contribution of GCs exposure to the R(t) dynamics	0.3
k_{RS}	Contribution of the inflammatory stimulus to the R(t) dynamics	0.4
δ_R	Decay rate of reduced GR sensitivity	0.7
X_{pre}	Initial value for administration 2 h before LPS: Xdose exp(-kel·2/24)	≈1.72

2.5. Numerical implementation of the model

The mathematical model was implemented, the numerical results were processed, and the figures were generated in Python using Google Colab. NumPy was used to work with arrays and model parameters, SciPy tools were used for numerical integration of the system of ordinary differential equations and computation of equilibrium states, and Matplotlib was used to visualize time courses, phase portraits, bifurcation diagrams, and sensitivity analysis results.

The system of ordinary differential equations was integrated as an initial-value problem with prescribed initial conditions. The initial conditions were defined according to the experimental design and the selected modeling scenario. For the baseline physiological state, the levels of peripheral and central inflammatory mediators, microglial activation, neural tissue damage, and reduced efficiency of glucocorticoid receptor-mediated signaling were set to zero. The initial value of the variable describing glucocorticoid exposure in the central pharmacokinetic compartment at the time of lipopolysaccharide administration was calculated with allowance for preventive drug administration 2 h before the inflammatory stimulus and subsequent drug elimination.

Integration was performed with the LSODA solver, which switches automatically between methods intended for non-stiff and for stiff problems [25,26], as implemented in the SciPy library [27]; the choice is dictated by the structure of the system, the ratio of the maximum to the minimum real part of the eigenvalues of the Jacobian matrix along the trajectory ranging from 3.9 to 8.3. The relative and absolute tolerances were set to 1×10^{-8} and 1×10^{-10}, respectively (10^{-10} and 10^{-12} in the verification runs), and the solution was stored on a uniform grid of 1201–2000 points over 0–30 days, or over a longer interval when the persistence of the chronic state was examined; runs for which the solver did not converge were discarded rather than reported.

The correctness of the numerical solution was verified separately. Comparison with the exact solutions of the subsystems that admit them—the exponential decay of lipopolysaccharide and of the central drug compartment and the biexponential solution of the effect compartment [28,29]—gave deviations of 1.2×10^{-13} to 8.7×10^{-13}, that is, at the level of round-off error; the observed order of accuracy of a fourth-order Runge–Kutta reference solution converged monotonically to four, five independent solvers (LSODA, Radau, BDF, DOP853, RK45) agreed to within 9.3×10^{-10}, and in 60 runs with random lipopolysaccharide doses, no violation of non-negativity or of the constraint $0 \leq Ma(t) \leq Ma_{max}$ was recorded. The accuracy achieved exceeds the error of the experimental data by seven or more orders of magnitude and therefore makes no contribution to the discrepancies between model and experiment.

Equilibrium states were determined by setting the right-hand sides of the system equal to zero. Two complementary procedures were used, and both were required to yield the same set: a multi-start hybrid Powell solution of the algebraic system from initial approximations distributed over the admissible range of the variables, and an exact reduction of the problem to a single scalar equation. In the latter, since the external inputs vanish at equilibrium ($L = X_c = X_e = C_{per} = 0$), the coordinates C_{brain}, D, and R are expressed through Ma by the closure relations and the problem reduces to solving $F(Ma) = 0$ on $[0; Ma_{max}]$; F was evaluated on a uniform grid of 20,000 nodes, and every root was refined by Brent's method [30] with a tolerance of 10^{-13}, which locates all equilibria simultaneously and excludes the loss of branches that continuation methods may suffer near a fold point. Roots differing in norm by less than 1×10^{-4} were merged and negative roots discarded as biologically inadmissible. The stability of each equilibrium was classified from the eigenvalues of the Jacobian matrix of the full

eight-dimensional system, evaluated by central differences.

Control parameters were the microglial sensitivity to central inflammatory mediators and the rate of production of central inflammatory mediators by activated microglia, that is, the two coefficients that define the gain of the central positive feedback circuit. The bifurcation diagrams were computed by varying η over the range 0.5–4.0 and β_{brain} over the range 0.2–2.5; in both cases, a uniform grid of 90 nodes was used, corresponding to step sizes of 0.039 and 0.026, respectively. The remaining parameters were fixed at the values of regime C with $D_{LPS} = 0$, and the complete set of equilibria and the corresponding eigenvalues was recomputed at every grid point.

The critical parameter values were determined independently of the step size of the diagram: the number of equilibria was used as an indicator function of the parameter, and the point at which it changes was located by bisection with a tolerance of 10^{-4}, then verified by directly solving the double-root condition $F(Ma) = 0$, $\partial F/\partial Ma = 0$, which corresponds to the tangency of the branches at a saddle-node point [31]. The two approaches agreed to within 1.5×10^{-5} ($\eta_{crit} = 2.2489$ versus 2.2488; $\beta_{brain,crit} = 1.2452$ versus 1.2452), and nine combinations of grid resolution and bisection tolerance gave a spread of no more than 1.3×10^{-4}.

The information content of the experimental data was assessed by principal component analysis [32] of a 24×4 matrix (condition × marker) after centering and scaling. The same method was applied to the matrix of model trajectories (3001×6) in order to estimate the effective dimensionality of the dynamics. Global sensitivity analysis was performed over a range of ±50% around the baseline values by three methods: Morris elementary effects screening (20 trajectories) [33], partial rank correlation coefficients on a Latin hypercube (1000 points) [34], and Sobol variance decomposition following the Saltelli scheme (6656 evaluations) [35].

3. Results and discussion

3.1. Well-posedness of the model

Before analyzing the equilibria, stability, and bifurcation transitions, it is necessary to establish that the constructed ODE system is mathematically well-posed. Specifically, for biologically admissible initial conditions, the solution must exist, be unique, remain non-negative, and not become unbounded within a finite time interval. These properties are particularly important for a biological model because all state variables have a specific physiological interpretation.

For the model to remain biologically meaningful, its solutions must preserve non-negativity whenever the initial conditions are non-negative. Consider the non-negative state space (16)

$$\Omega = \{Y \in R_+^8 : L, X_c, X_e, C_{per}, C_{brain}, Ma, D, R \geq 0\} \tag{16}$$

Let U be the open set in $\mathbb{R}^8$ defined by the conditions $C_{per} > -K_{BBB}$, $D > -K_D$ and by the positivity of $1 + \alpha_C R$ and $1 + \alpha_N R$; it contains the non-negative orthant Ω. On U, the right-hand side of the final system is of class C^∞, since all of its components are sums, products, and quotients of polynomials and rational functions whose denominators are bounded away from zero, the evenness of the exponents $m = 2$, $n = 4$, $q = r = 2$, guaranteed for the Hill-type terms. By the Picard–Lindelöf theorem [36], the Cauchy problem, therefore, has a unique solution on a maximal interval $[0, t_{max})$ for any $y_0 \in U$.

The non-negative orthant is positively invariant, which follows from the quasi-positivity of the right-hand side [37,38]: when any coordinate vanishes, only influx terms remain in the corresponding component, so that $dC_{brain}/dt = \beta_{brain} Ma + J(C_{per}) \geq 0$ at $C_{brain} = 0$, $dMa/dt \geq 0$ at $Ma = 0$, $dD/dt =$

$k_{in}C_{brain} \geq 0$ at D = 0, and similarly for the remaining variables. No model variable can therefore take a negative value.

The solutions are bounded by explicit constants obtained successively by the comparison lemma [39]: L and X_c decay exponentially, $X_e \leq \max\{X_e(0), X_c(0)\}$, boundedness of σ_L by σ_{max} bounds C_{per}, negativity of the right-hand side at $Ma = Ma_{max}$ makes the interval $[0, Ma_{max}]$ invariant, and boundedness of the flux across the barrier then bounds C_{brain}, D, and R in turn. These bounds define a compact positively invariant absorbing set, so that the solution is continued to the whole half-line, $t_{max} = +\infty$, and continuity of the derivative of the right-hand side on that set together with Grönwall's lemma gives continuous dependence on the initial data and on the parameters. The problem is thus well-posed in the sense of Hadamard [40], and the biological interpretation of all state variables is preserved.

3.2. Equilibria of the system

One of the key stages in investigating the dynamic properties of a mathematical model is the analysis of its equilibria. From a biological perspective, equilibria represent persistent functional regimes of the neuroimmune system toward which the system, and therefore the organism, evolves after an inflammatory challenge. The equilibria are determined by the condition (17)

$$\frac{dY}{dt} = 0 \tag{17}$$

The first equations of the system imply

$$-\delta_L L^* = 0 \quad \Rightarrow \quad L^* = 0, \qquad -k_{el}X_c^* = 0 \quad \Rightarrow \quad X_c^* = 0.$$

$$k_{e0}(X_c^* - X_e^*) = 0 \quad \Rightarrow \quad X_e^* = 0.$$

Since the external LPS and glucocorticoid inputs vanish at equilibrium, the peripheral cytokine equation reduces to $-\delta_{per}C_{per}^* = 0$, and therefore, $C_{per}^* = 0$. Consequently, every equilibrium of the complete system has the form (18)

$$E^* = (0,0,0,0, C_{brain}^*, Ma^*, D^*, R^*) \tag{18}$$

For convenience, define

$$\delta_b = \delta_{brain}^{eff}(D_{LPS}), k_d = k_{in}^{eff}(D_{LPS}), k_d = k_{in}^{eff}(D_{LPS}), \eta_d = \eta^{eff}(D_{LPS}), \rho_d = \rho^{eff}(D_{LPS})$$

At equilibrium, $I_C(0, R^*) = 1, I_N(0, R^*) = 1$

The equation for central inflammatory mediators becomes $0 = \beta_{brain}Ma^* - \delta_b C_{brain}^*$, which gives $C_{brain}^* = \frac{\beta_{brain}}{\delta_b}Ma^*$. From the damage equation $0 = k_d C_{brain}^* - k_{out}D^*$, we obtain $D^* = \frac{k_d}{k_{out}}C_{brain}^* = \frac{k_d\beta_{brain}}{k_{out}\delta_b}Ma^*$. The central inflammatory stimulus at equilibrium is defined as $stim_0^* = \eta_d C_{brain}^* + \rho_d \frac{D^*}{K_D + D^*}$. Substituting the expressions for C_{brain}^* and D^* gives $g(Ma^*) = \eta_d \frac{\beta_{brain}}{\delta_b}Ma^* + \rho_d \frac{\frac{k_d\beta_{brain}}{k_{out}\delta_b}Ma^*}{K_D + \frac{k_d\beta_{brain}}{k_{out}\delta_b}Ma^*}$, $where\ h(g) = \frac{g^n}{K^n + g^n}$ .The equilibrium equation for activated microglia can therefore be written as (19)

$$(Ma^*) = 0 \tag{19}$$

Where $F(Ma) = \kappa_{in} h(g(Ma))(Ma_{max} - Ma) - \kappa_{out} Ma.$

Thus, determining the equilibria of the complete eight-dimensional system is reduced to solving the single nonlinear equation (20)

$$F(Ma^*) = 0, \text{with respect to } Ma^* \tag{20}$$

Once Ma^* has been determined, the remaining components of the equilibrium are calculated as (21)

$$C^*_{brain} = \frac{\beta_{brain}}{\delta_b} Ma^*, D^* = \frac{k_d}{k_{out}} C^*_{brain} = \frac{k_d \beta_{brain}}{k_{out} \delta_b} Ma^*, R^* = \frac{k_{RS}}{\delta_R} \frac{(g(Ma^*))^r}{K_R^r + (g(Ma^*))^r} \tag{21}$$

The system always possesses the trivial equilibrium (22)

$$E_0 = (0,0,0,0,0,0,0,0) \tag{22}$$

Biologically, this state corresponds to the absence of circulating pro-inflammatory cytokines, microglial activation, accumulated neural tissue damage, and residual inflammatory signaling.

This regime represents the most favorable outcome of neuroinflammation and corresponds to the normal functioning of the body's protective mechanisms, in which the inflammatory response performs its defensive role and subsequently resolves spontaneously.

For certain parameter values, the system may also possess a nontrivial equilibrium (23):

$$E^* = (0,0,0, C^*_{brain}, Ma^*, D^*, R^*), \text{ where } C^*_{brain} > 0, Ma^* > 0, D^* > 0, R^* > 0, C^*_{Per} = 0 \tag{23}$$

In this state, peripheral inflammation has completely resolved, while a self-sustaining inflammatory feedback circuit persists within the CNS. Even after complete elimination of lipopolysaccharide from the body and cessation of the peripheral inflammatory signal, the system retains activated microglia, elevated levels of central inflammatory mediators, accumulated neural tissue damage, and altered sensitivity of the glucocorticoid regulatory pathway.

Thus, the inflammatory process becomes independent of the initial trigger and is maintained by the internal positive feedback mechanisms incorporated into the model. The central mediator–microglia feedback circuit plays the principal role: central inflammatory mediators activate microglia, which in turn produce additional inflammatory mediators. When the overall amplification within this loop exceeds the capacity of the system to eliminate inflammatory signals, a stable chronic state emerges.

Biologically, the nontrivial equilibrium may be interpreted as a state of persistent low-grade neuroinflammation that remains after the initial damaging stimulus has been removed. Similar processes have been described in a range of neurodegenerative and neuroimmune disorders, including Alzheimer's disease, Parkinson's disease, the long-term consequences of traumatic brain injury, and chronic neuroimmune conditions [1,2,20].

The existence of multiple equilibria provides the basis for bistability and bifurcation transitions. Depending on the parameter values, the system may either return to the physiological state or shift to a chronic inflammatory regime. This behavior reflects the biologically meaningful transition from a reversible inflammatory response to a self-sustaining chronic inflammatory state when the inflammatory stimulus is sufficiently strong or prolonged.

3.3. Linearization and Jacobian matrix

The local dynamics of the final ODE model are determined by the 8 × 8 Jacobian matrix, which contains all first-order partial derivatives of the right-hand sides of the system with respect to the state variables (24):

$$J(Y^*) = \left(\frac{\partial f_i}{\partial x_j}\right) \tag{24}$$

The Jacobian matrix, for the present model, has the form (25)

$$J = \begin{pmatrix} \frac{\partial f_1}{\partial L} & \frac{\partial f_1}{\partial X_c} & \cdots & \frac{\partial f_1}{\partial R} & \frac{\partial f_2}{\partial L} & \frac{\partial f_2}{\partial X_c} & \cdots & \frac{\partial f_2}{\partial R} \\ \vdots & \vdots & \ddots & \vdots & \vdots & \vdots & \ddots & \vdots \\ \frac{\partial f_8}{\partial L} & \frac{\partial f_8}{\partial X_c} & \cdots & \frac{\partial f_8}{\partial R} \end{pmatrix} \tag{25}$$

The Jacobian matrix is of dimension 8 × 8.

3.4. Eigenvalue-based stability analysis

Consider the trivial equilibrium $E_0 = (0,0,0,0,0,0,0,0)$. At this point, all inflammatory processes are absent. The Jacobian matrix has a block-triangular structure. The eigenvalues associated with the linear subsystems are obtained directly: $\lambda_1 = -\delta_L, \lambda_2 = -k_{el}, \lambda_3 = -k_{e0}, \lambda_4 = -\delta_{per}$, $\lambda_8 = -\delta_R$. All these eigenvalues are negative because they correspond to clearance, elimination, and degradation processes. For the central subsystem (C_{brain}, Ma, D), the Jacobian block takes the form (26)

$$A = \begin{pmatrix} -\delta_{brain} & \beta_{brain} & 0 & 0 \\ -\kappa_{out} & 0 & k_{in}^{eff} & 0 \\ -k_{out} \end{pmatrix} \tag{26}$$

Since this matrix is triangular, its eigenvalues are given by $\lambda_5 = -\delta_{brain}, \lambda_6 = -\kappa_{out}$, $\lambda_7 = -k_{out}$. Therefore, $\lambda_i < 0, \ \forall i$.

Thus, the trivial equilibrium E_0 is locally asymptotically stable. Its stability indicates that, following a sufficiently small inflammatory perturbation, the system is able to return spontaneously to the physiological state. Although C_{brain}, Ma, D may increase transiently, all variables gradually decay after elimination of LPS and activation of the clearance mechanisms. Biologically, this behavior corresponds to normal resolution of the inflammatory response.

Consider the nontrivial steady state $E_+ = (0,0,0,0, C^*_{brain}, Ma^*, D^*, R^*)$. Unlike E_0, this state is characterized by nonzero levels of central inflammatory mediators, activated microglia, and accumulated tissue damage. The feedback loop $C_{brain} \rightarrow Ma \rightarrow D \rightarrow Ma$ remains active at steady state. Consequently, the Jacobian matrix contains additional derivatives of the Hill function and the saturating regulatory functions. For the parameter set identified through the bifurcation analysis, the following eigenvalues were obtained:

$$\lambda = \{-2.736, -1.800, -1.647, -1.400, -1.200, -1.160, -1.000, -0.700\}.$$

All eigenvalues are real and negative; therefore, $R(\lambda_i) < 0, \ \forall i$. Hence, the nontrivial steady state E_+ is locally asymptotically stable.

The stability of this state indicates that, once chronic neuroinflammation has developed, it becomes self-sustaining. Even after complete elimination of the initial LPS stimulus, the system does not return automatically to the physiological state. Small perturbations are insufficient to disrupt the established inflammatory feedback circuit, and after a deviation from the equilibrium, the system

returns to E_+. Biologically, this behavior corresponds to a stable chronic inflammatory regime.

The coordinates of the equilibria of the final ODE system and the corresponding eigenvalues of the Jacobian matrix are presented in Tables 4 and 5.

Table 4. Coordinates of the equilibria of the final ODE model.

Equilibrium	L*	Xc*	Xe*	C_{per}*	C_{brain}*	Ma*	D*	R*	Biological interpretation
E_0	0	0	0	0	0	0	0	0	Trivial physiological equilibrium
E_1	0	0	0	0	0.254	0.442	0.077	0.296	Intermediate threshold equilibrium
E_+	0	0	0	0	0.560	0.975	0.169	0.479	Stable nontrivial chronic equilibrium

Table 5. Eigenvalues of the Jacobian matrix evaluated at the equilibria.

Equilibrium / subsystem	Eigenvalues/spectral condition	Stability classification
E_0 (physiological equilibrium)	$(-\delta_L, -k_{el}, -k_{e0}, -\delta_{per}, -\delta_{brain}, -\delta_{Ma}, -\delta_D, -\delta_R)$; all are negative for positive rate constants	Locally asymptotically stable physiological node
E_1 (intermediate threshold equilibrium)	One eigenvalue has Re(λ) > 0, whereas the remaining seven eigenvalues have Re(λ) < 0; the numerical spectrum should be reported directly from the computational output	Saddle (unstable threshold equilibrium and basin boundary)
E_+ (chronic equilibrium)	(−2.736, −1.800, −1.647, −1.400, −1.200, −1.160, −1.000, −0.700)	Locally asymptotically stable nontrivial chronic node
Spectral decomposition for E_+	Central nonlinear block: (−2.736, −1.647, −1.160); linear PK, elimination, and clearance directions: (−1.800, −1.400, −1.200, −1.000, −0.700)	All directions are exponentially stable

For E_0, the eigenvalues are reported analytically because the block-triangular structure makes their signs explicit for positive rate constants. For E_+, the complete numerical spectrum contains eight negative real eigenvalues. The three values −2.736, −1.647, and −1.160 correspond to the central nonlinear inflammatory block, whereas −1.800, −1.400, −1.200, −1.000, and −0.700 arise from the linear pharmacokinetic, elimination, and clearance directions. For E_1, the available calculation establishes the saddle signature (one positive and seven negative real parts), but a numerical spectrum should only be inserted from the original computational output. The stability results are further supported by the phase portraits shown in Figure 2.

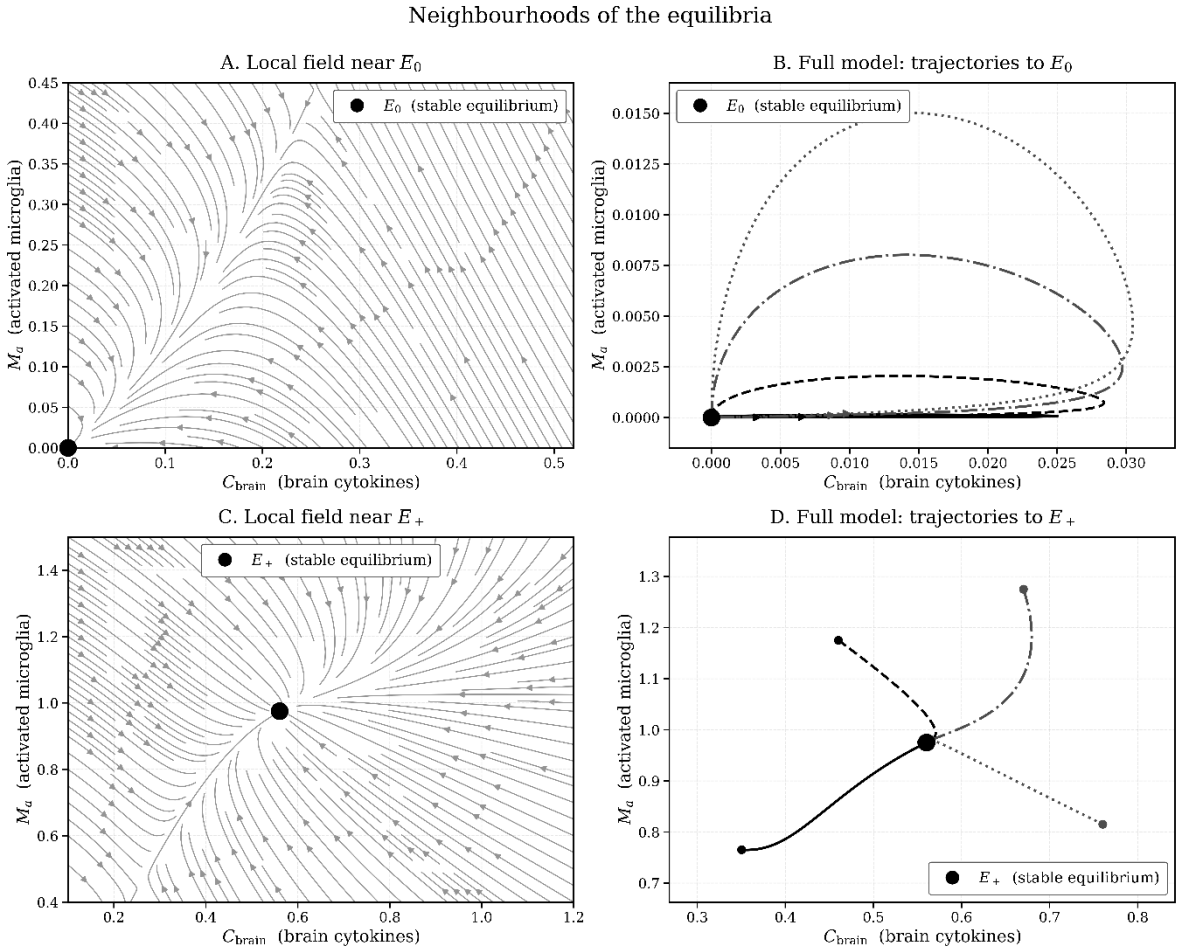

Figure 2. Phase-plane analysis of the neuroinflammation model. (A) Phase portrait near the stable trivial equilibrium E_0 . The vector field and representative trajectories demonstrate convergence to the baseline state. (B) Phase trajectories of the full model obtained from different initial conditions and converging to E_0, corresponding to resolution of neuroinflammation. (C) Phase portrait near the unstable nontrivial equilibrium E_1. Trajectories approach E_1 only along its stable direction and diverge following perturbations along unstable directions. (D) Full-model trajectories in the vicinity of E_1, illustrating its threshold-like role in separating distinct dynamical outcomes. C_{brain} denotes the brain cytokine level, and Ma denotes activated microglia.

Between the two stable equilibria E_0 and E_+ lies the intermediate equilibrium E_1. Its Jacobian has one eigenvalue with a positive real part and seven eigenvalues with negative real parts; therefore, E_1 is a saddle point. This spectral signature is consistent with its role as an unstable threshold equilibrium.

This equilibrium is not observed as a stable dynamical regime; its stable manifold forms the separatrix between the basins of attraction of the physiological and the chronic equilibria and, therefore, represents the critical threshold for the transition to chronic neuroinflammation. If the initial perturbation remains below it, the system returns to the physiological equilibrium, whereas if it is exceeded, the trajectory evolves toward the chronic state. The coexistence of two stable equilibria

separated by a saddle is a classical indication of bistability, which motivates the bifurcation study that follows.

3.5. Bifurcation analysis

The purpose of the bifurcation analysis is to identify the parameters whose variation produces qualitative changes in the number or stability of the equilibria, and hence the conditions under which the system shifts from physiological resolution of inflammation to a self-sustaining chronic state after the initial LPS stimulus has disappeared.

The final neuroinflammation model contains a relatively large number of parameters; however, they do not contribute equally to the transition toward chronic inflammation. Analysis of the system structure indicates that the positive feedback circuit $C_{brain} \to Ma \to C_{brain}$ plays a central role. This loop can maintain inflammation even after the initial LPS stimulus has been eliminated.

Two parameters are particularly important within this feedback mechanism. The first is η, which enters the expression for the central inflammatory stimulus, $stim_0 = \tilde{\delta}L + \eta^{eff} C_{brain} + \rho^{eff} \frac{D}{K_D+D}$, and characterizes microglial sensitivity to central inflammatory mediators. Higher values of η result in stronger stimulation of microglial activation by central inflammatory mediators.

The second parameter is β_{brain}, which appears in the equation for central inflammatory mediators: $\frac{dC_{brain}}{dt} = \beta_{brain} Ma + J_{BBB} - \delta_{brain}^{eff} C_{brain}$. This parameter determines the rate at which activated microglia produce central inflammatory mediators. Thus, η describes the pathway $C_{brain} \to Ma$, and β_{brain} $Ma \to C_{brain}$. Together, these processes form a closed positive feedback circuit. By contrast, δ_{brain} represents the clearance of central inflammatory mediators and, therefore, counteracts the amplification of this loop.

The bifurcation analysis was performed using the reduced equilibrium system obtained after eliminating the rapidly decaying variables: $L^* = X_c^* = X_e^* = C_{per}^* = 0$.

Accordingly, the long-term behavior of the system is determined by the central subsystem (C_{brain}, Ma, D, R).

The equilibria were determined from the following nonlinear equation with respect to (27):

$$F(Ma) = \kappa_{in} h(g(Ma))(Ma_{max} - Ma) - \kappa_{out} Ma \tag{27}$$

where $C_{brain}^* = \frac{\beta_{brain}}{\delta_b} Ma^*, D^* = \frac{k_d}{k_{out}} C_{brain}^* = \frac{k_d \beta_{brain}}{k_{out} \delta_b} Ma^*, R^* = \frac{k_{RS}}{\delta_R} \frac{(g(Ma^*))^r}{K_R^r + (g(Ma^*))^r}$

For each identified equilibrium, the Jacobian matrix of the complete system was constructed and its eigenvalues were calculated. An equilibrium was classified as locally asymptotically stable when $\mathrm{Re}(\lambda i) < 0$ for every eigenvalue. It was classified as a saddle when at least one eigenvalue had a positive real part and at least one had a negative real part. This criterion was applied consistently to the physiological equilibrium E_0, the intermediate threshold equilibrium E_1, and the chronic equilibrium E_+. If at least one eigenvalue had a positive real part, the equilibrium was classified as unstable.

The parameters η and β_{brain} were selected as bifurcation parameters because they characterize the strength of the central positive feedback circuit $Ma \to C_{brain} \to D \to stim \to Ma$. This loop represents the mechanism responsible for the self-sustaining nature of the neuroinflammatory process: activated microglia enhance the production of central inflammatory mediators, these mediators promote tissue damage, and the accumulated damage further supports microglial activation.

Variation of the first bifurcation parameter showed that, at low parameter values, the system possesses a single stable physiological equilibrium. At a critical parameter value, a pair of positive equilibria—one saddle and one stable chronic equilibrium—emerges through a saddle-node bifurcation. The physiological equilibrium remains locally stable, and the coexistence of E_0 and E_+ produces a bistable regime separated by the stable manifold of E_1.

A similar result was obtained for the second bifurcation parameter. Below its critical value, only the stable physiological equilibrium is present. At the critical value, a saddle-node bifurcation creates two additional positive equilibrium branches: an unstable intermediate branch E_1 and a stable chronic branch E_+. Thus, the transition is characterized by the emergence of bistability rather than by a loss of stability of E_0. The corresponding numerical estimates are presented in Table 6.

Table 6. Critical parameter values identified by bifurcation analysis.

Parameter	Critical value	Biological interpretation
η_{crit}	2.26	Saddle-node creation of an unstable threshold equilibrium and a stable chronic equilibrium; onset of bistability while the physiological equilibrium remains stable
$\beta brain_{crit}$	1.25	Saddle-node onset of the self-sustaining microglia-mediator feedback regime and coexistence of physiological and chronic attractors

The obtained results indicate that, within the model, neuroinflammation does not necessarily progress to a chronic state after every inflammatory stimulus. When the central positive feedback is weak, the system returns to the physiological state. However, when the parameters governing inflammatory self-maintenance exceed their critical values, a stable nonzero equilibrium becomes possible. This corresponds to a scenario in which persistent microglial activation and elevated levels of central inflammatory mediators sustain the inflammatory process even after the initial peripheral stimulus has disappeared.

In the bifurcation diagrams (Figure 3), stable equilibria are indicated by filled circles, whereas unstable equilibria are marked by crosses. Below the saddle-node threshold, only the stable physiological branch exists. At the critical value, a stable and an unstable positive branch are created as a pair. Beyond this threshold, the physiological and chronic equilibria coexist, and the unstable intermediate branch defines the boundary between their basins of attraction.

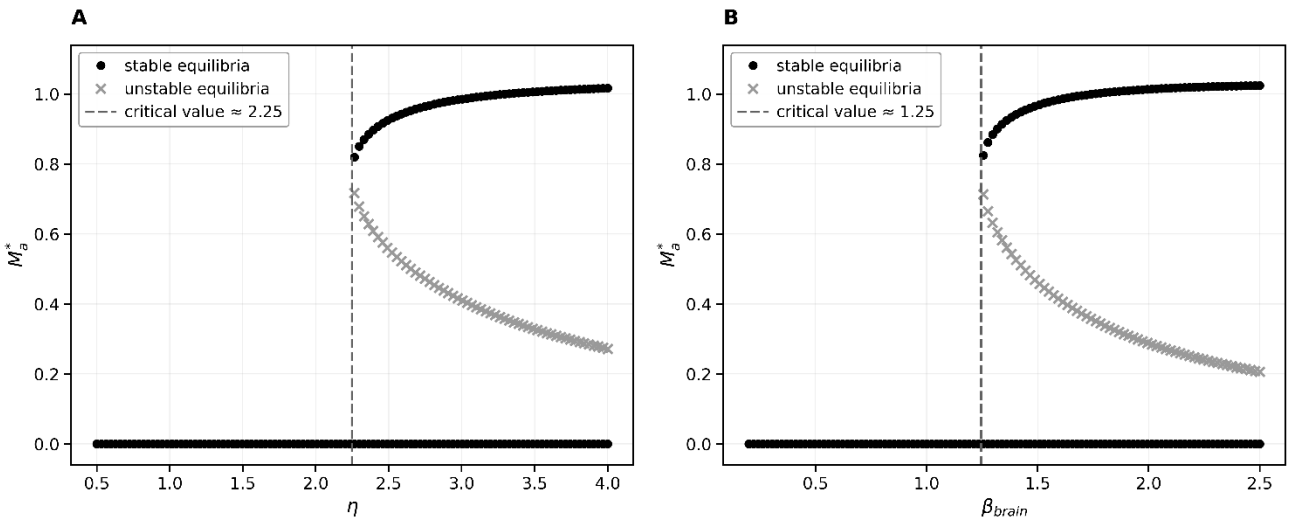

Figure 3. Bifurcation diagram of equilibrium states with respect to η (A), β_{brain} (B).

Stable equilibria are indicated by filled circles, whereas unstable equilibria are marked by crosses. Below the critical value of the control parameter, only the stable zero branch exists. After the critical value is crossed, two positive branches emerge, indicating the appearance of a threshold mechanism for chronic inflammation.

The bifurcation is a non-degenerate saddle-node (fold) bifurcation: at the critical point, the Jacobian matrix has a simple zero eigenvalue with seven negative ones, the normal-form coefficient and the derivative with respect to the parameter are non-zero, and the divergence of the branches follows a square-root law with an exponent of 0.499 against the theoretical value of 0.5. Computational details are given in Subsection 2.5.

3.6. Parameter regions and dynamic regimes of the model

Bifurcation analysis showed that variation in the parameters governing the strength of the central positive feedback circuit gives rise to qualitatively distinct patterns of system behavior. The baseline parameter values and the methods used for their determination are presented in the Materials and Methods section, whereas the present section focuses on parameter combinations associated with different dynamical regimes of neuroinflammation.

Three characteristic regions of parameter space were identified, corresponding to distinct scenarios of inflammatory progression: Regime A, rapid resolution of inflammation; Regime B, delayed recovery with prolonged persistence of central inflammatory alterations; and Regime C, bistability and a threshold-dependent transition between the physiological and chronic states. For each regime, a representative parameter set was selected on the basis of the bifurcation structure of the system, the stability of the equilibrium states, and the behavior of the numerical trajectories. The corresponding parameter sets are presented in Table 7.

Table 7. Parameter sets defining the dynamic regimes identified by bifurcation analysis.

Parameter	Regime A	Regime B	Regime C
β_{brain}	0.40	0.50	1.538
H	0.60	1.10	2.863
ρ	0.20	0.25	2.103
k_{BBB}	0.12	0.06	0.30
δ_{brain}	3.00	0.85	2.677
κ_{in}	1.00	0.95	2.258
κ_{out}	1.00	0.24	1.179

Considering several parameter regimes makes it possible to analyze not only a single baseline solution but also qualitatively distinct scenarios of inflammatory progression. A similar approach has been used in mathematical models of neuroinflammation to distinguish resolving, sustained pro-inflammatory and insufficient reparative responses, as well as to investigate transitions between physiological and chronic pathological states [18,19].

In the present study, Regimes A, B, and C represent different balances among activation of the inflammatory feedback circuit, resolution mechanisms, and the effects of glucocorticoids. In Regime A, the system converges to the stable zero equilibrium: the inflammatory system responds to the stimulus and returns to the physiological baseline once it has been eliminated. In Regime B, the system also returns asymptotically to the zero equilibrium, but the spectrum of the Jacobian matrix contains eigenvalues close to zero ($\lambda_{slow} \approx -0.2 \ldots -0.35$), so that the central variables retain a prolonged positive tail after the peripheral response has resolved; this regime most closely reflects the experimentally observed persistence of neuroinflammatory features. In Regime C, the central positive feedback is strong enough for two stable equilibria to coexist, separated by an unstable intermediate one: a weak initial perturbation decays, whereas a sufficiently strong one drives the system to the chronic state, which indicates a critical threshold for the transition to chronic neuroinflammation. The characteristics and biological interpretation of the regimes are summarized in Table 8.

Table 8. Dynamic regimes of the model and their biological interpretation.

Regime	Mathematical characterization	Biological interpretation
A: Stable zero state	E_0 is stable; all Re(λi) < 0; rapid return to zero	An acute LPS challenge initiates inflammation, after which the system returns to baseline
B: Stable zero state with delayed inflammatory resolution	E_0 is stable; several eigenvalues are negative and small in magnitude	The peripheral response decays rapidly, whereas central variables retain a prolonged tail
C: Bistability/threshold for chronicity	E_0, E_1, and E_+ coexist; E_0 and E_+ are stable, whereas E_1 is an unstable threshold state	Small perturbations decay, whereas sufficiently strong perturbations shift the system to a chronic self-sustaining state

To further support the results of the stability analysis, phase portraits of the system were constructed in the C_{brain} and Ma plane. This projection was chosen because the interaction between

central inflammatory mediators and microglia forms the principal self-sustaining feedback circuit of neuroinflammation $C_{brain} \rightarrow Ma \rightarrow C_{brain}$.

In the stable zero regime, all phase trajectories converge to the point $(C^*_{brain}, Ma^*) = (0,0)$.

In the stable nontrivial regime, the trajectories converge to a nonzero equilibrium point, $C^*_{brain}, Ma^*) \neq (0,0)$.

In the bistable regime, the phase space is divided into two basins of attraction, $B(E_0)$ and $B(E_+)$. The boundary between them corresponds to the threshold level of central activation beyond which the system no longer returns to the zero state but instead evolves toward the chronic inflammatory state. The corresponding phase trajectories are shown in Figure 4.

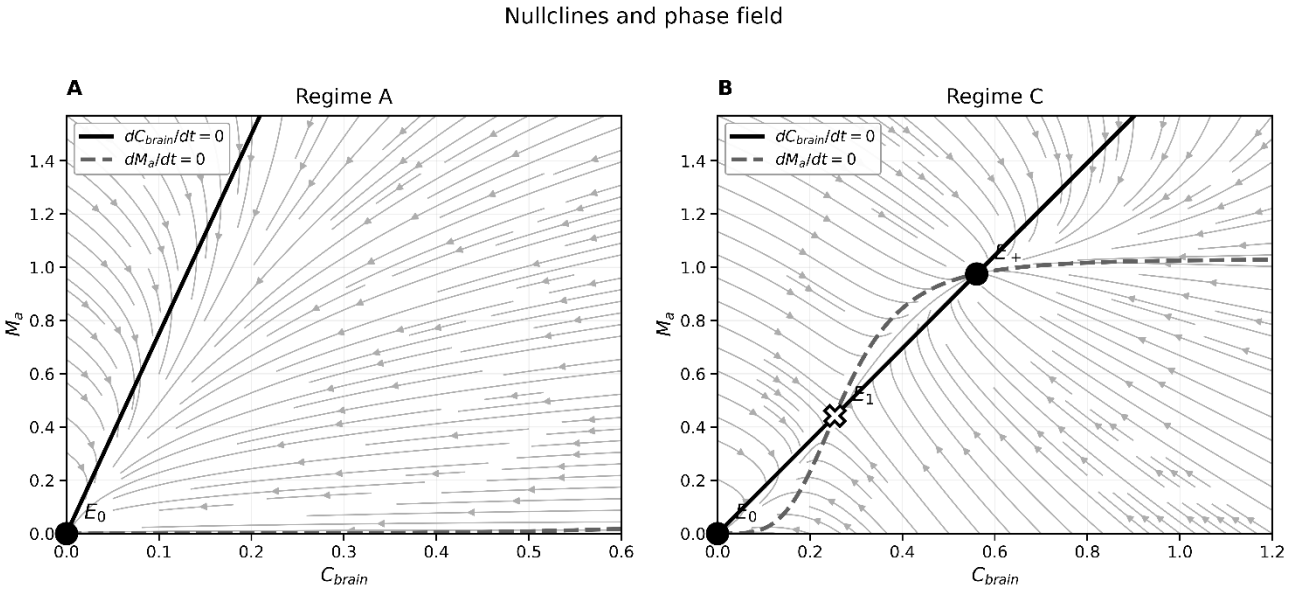

Figure 4. Nullclines and phase fields for regimes A–C in the (C_{brain}, Ma) plane. Regime A: The intersection of the nullclines defines the unique equilibrium. The vector field shows that all trajectories converge to this point, confirming its stability and the resolution of the inflammatory response. Regime C. The physiological equilibrium E_0 and the chronic equilibrium E_+ are stable and possess distinct basins of attraction. The intermediate equilibrium E_1 is a saddle point. Its separatrix forms the threshold between recovery and transition to a self-sustaining chronic neuroinflammatory state.

3.7. Sensitivity analysis

The bifurcation analysis identified the parameters capable of qualitatively changing the operating regime of the system and shifting it from resolving inflammation to chronic neuroinflammation. However, bifurcation analysis does not quantify the relative influence of individual parameters on the magnitude of the inflammatory response.

To identify the parameters governing the transition from a resolving inflammatory response to a stable chronic neuroinflammatory regime, a local sensitivity analysis of the ODE system was performed at $\eta = 2.35$, slightly above the bifurcation threshold $\eta crit \approx 2.26$, using a ±5% one-at-a-time perturbation of each parameter. The primary outcome measure was the area under the curve of central pro-inflammatory mediators over the 0–30-day interval (28):

$$Y_{AUC} = \int_0^{30} Cbrain(t)dt \tag{28}$$

Additional outcome measures included the peak magnitude of central inflammation, the cumulative activation of microglia, and the cumulative neural tissue damage (29):

$$Y_{peak} = max_{0\le t\le 30} C_{brain}(t)\,,\ AUC_{Ma} = \int_0^{30} Ma(t)dt\,,\ AUC_D = \int_0^{30} D(t)dt \tag{29}$$

The ODE system was integrated over 0–30 days. For the baseline trajectory, AUC (C_{brain}) = 0.5084, Peak (C_{brain}) = 0.1293, AUC (Ma) = 0.1833, and AUC (D) = 0.1537. For calculations in or near the bistable regime, perturbed trajectories were checked to ensure that they remained in the same basin of attraction as the baseline trajectory; perturbations crossing the separatrix were classified as regime changes rather than local sensitivities. The normalized sensitivity coefficient was calculated as (30):

$$S_i = \frac{\left(Y(p_i \cdot 1.05) - Y(p_i \cdot 0.95)\right)}{(0.1 \cdot Y_0\ ).} \tag{30}$$

where (Y_0) is the value of the selected outcome measure at the baseline parameter set.

Table 9. Normalized local sensitivity coefficients.

Parameter	Biological meaning	S(AUC(C_{brain}))	S(Peak(C_{brain}))	S(AUC(Ma))	S(AUC(D))
K	Microglial activation threshold	−1.879	−1.861	−7.887	−1.879
δ_{brain}	Central inflammatory mediator clearance rate	−1.619	−1.379	−2.562	−1.619
k_{BBB}	Peripheral-to-brain BBB coupling	1.337	1.226	2.414	1.337
η	Microglial sensitivity to central mediators	0.717	0.641	3.010	0.717
δ_{per}	Peripheral cytokine clearance rate	−0.662	−0.169	−0.434	−0.662
δ_{L}	LPS clearance rate	0.516	0.365	0.821	0.516
β_{brain}	Microglial production of central mediators	0.448	0.462	0.880	0.448
κ_{in}	Microglial activation rate	0.436	0.449	1.832	0.436
κ_{out}	Microglial deactivation rate	−0.361	−0.293	−1.518	−0.361
ρ	Contribution of damage to microglial activation	0.078	0.053	0.326	0.078
k_{in}	Damage accumulation rate	0.076	0.052	0.320	1.076
k_{out}	Damage repair/resolution rate	−0.046	−0.021	−0.192	−1.048

A positive value of (S_i) indicates that increasing the parameter increases the selected outcome measure, whereas a negative value indicates that increasing the parameter decreases it. The resulting sensitivity coefficients are presented in Table 9 and visualized as a heat map in Figure 5.

The coefficients in Table 9 were calculated around the same baseline trajectory described above.

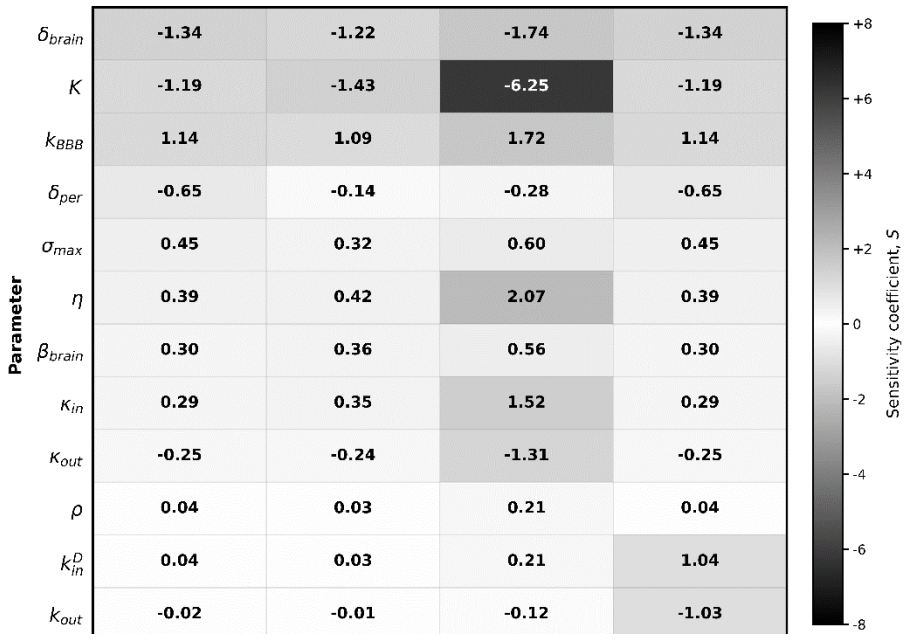

Figure 5. Heat map of the normalized sensitivity coefficients for the final model.

Taken together, the largest absolute sensitivities for AUC (C_{brain}) were observed for K (−1.879), δbrain (−1.619), BBB coupling (1.337), and η (0.717). These results quantitatively support the dominant role of the central mediator–microglia feedback circuit and the peripheral-to-central inflammatory bridge.

The sensitivity analysis should be interpreted together with the preceding bifurcation analysis. Bifurcation analysis identifies parameter changes that alter the qualitative operating regime of the system, whereas local sensitivity analysis quantifies the response to small perturbations within a fixed dynamical branch. Accordingly, the coefficients reported here characterize the neighborhood of the selected baseline trajectory and should not be extrapolated across the saddle-node threshold or across the separatrix between the physiological and chronic basins of attraction.

Thus, η and β_{brain} may be regarded as bifurcation-control points, whereas K and δ_{brain} are the most sensitive local regulators of inflammatory burden. The numerical sensitivity results reinforce the conclusion that chronic neuroinflammation is governed by the balance between positive central feedback, BBB-mediated input, activation threshold, and central mediator clearance.

3.8. Global sensitivity analysis and information content of the experimental data

The first two principal components of the experimental data account for 92.6% of the variance (83.3% and 9.3%). The first combines all four markers with similar loadings (0.487–0.522) and reflects the overall magnitude of the inflammatory response; the second contrasts the cytokine component with

the cellular one (TNF-α −0.645 versus IBA-1 0.617). The number of significant axes of variability coincides with the number of model variables describing the measured quantities.

For the model trajectories, the first two components account for 95.9% and the first three for 99.87% of the variability, the second component practically coinciding with lipopolysaccharide elimination (loading 0.882). The eight-dimensional system, therefore, evolves on a two-dimensional manifold, which justifies the phase-portrait projection used above.

Global sensitivity analysis confirmed the leading role of the microglial activation threshold K and of the clearance of central mediators δ_{brain}: they rank first and second by all the methods applied (μ^* = 18.90 and 16.03; PRCC −0.799 and −0.737; total Sobol indices 0.451 and 0.406). The sum of the first-order indices was 0.499 against a sum of total indices of 1.571, that is, about half of the variance of the outcomes is determined by parameter interactions. For η and k_{BBB}, the first-order indices are close to zero (0.004 and −0.002), while the total indices are 0.172 and 0.114. These parameters influence the outcome exclusively through interactions with others, which is not revealed by local analysis.

3.9. Calibration against the experimental data

Calibration was performed not as a full parametric identification of the system but as a quantitative link between the observed experimental trends and the model variables: two time points (48 h and 10 days) and the aggregated nature of the variables do not allow all coefficients to be identified.

Because the model variables do not correspond to single biomarkers, the data were converted into aggregated indices. Group means of IL-1β, TNF-α, iNOS, and IBA-1 were normalized to the corresponding control separately for each time point t, brain structure r, and marker m (31):

$$Y_{norm(g,t,r,m)} = Y_{mean(g,t,r,m)} / Y_{mean(Control,t,r,m)} \quad (31)$$

so that the control value equals 1. The calibration targets were defined as (32)

$$Cbrain_{exp} = (IL1\beta_{norm} + TNF\alpha_{norm} + iNOS_{norm})/3,\ Ma_{exp} = IBA1_{norm}, \quad (32)$$

$$D_{hist} = n_{positive}/n_{total}$$

where $n_{positive}$ is the number of animals (of n_{total} = 5) showing acidophilic necrosis, chromatolysis, or reduced cellularity. $Cbrain_{exp}$ thus represents the cytokine–nitrosative component as a whole rather than any single mediator; D_{hist} serves as semi-quantitative confirmation of morphological damage rather than a direct equivalent of D(t). The variables R(t), I_C, and I_N have no direct experimental counterpart.

The effect of preventive GCS administration was quantified relative to the LPS group (33),

$$\text{Reduction X (\%)} = ((X_{LPS} - X_{GCS+LPS}) / X_{LPS}) \times 100\% \quad (33)$$

where X is $Cbrain_{exp}$, Ma_{exp}, or D_{hist}; positive values indicate attenuation of the response. The corresponding values are given in Table 10.

Table 10. Relative decrease in the central inflammatory and microglial indices in the GCS+LPS groups compared with the LPS group.

Time	Structure	Group	Decrease in $Cbrain_{exp}$, %	Decrease in Ma_{exp}, %
48 h	PFC	Dex + LPS	27.7	27.4
48 h	PFC	MP + LPS	23.7	31.5
48 h	Hippocampus	Dex + LPS	22.3	22.8
48 h	Hippocampus	MP + LPS	20.1	33.9
10 days	PFC	Dex + LPS	20.5	14.4
10 days	PFC	MP + LPS	22.8	18.1
10 days	Hippocampus	Dex + LPS	7.3	9.0
10 days	Hippocampus	MP + LPS	11.2	18.2

At 48 h, the suppression was incomplete ($Cbrain_{exp}$ 20.1%–27.7%, Ma_{exp} 22.8%–33.9%); by day 10, it was weaker, particularly in the hippocampus ($Cbrain_{exp}$: 7.3% for Dex + LPS, 11.2% for MP + LPS).

Since the model variables have a zero physiological baseline, whereas the experimental indices are normalized to control, the observation mapping $Cbrain_{exp} \approx 1 + s_C \cdot Cbrain_{model}$, $Ma_{exp} \approx 1 + s_M \cdot Ma_{model}$, $D_{hist} \approx s_D \cdot D_{model}$ was used; the scaling factors s_C, s_M, and s_D do not alter the structure of the ODE model. For each parameter set θ, the system was integrated, model values were extracted at day 2 (48 h) and day 10, and the objective function (34)

$$J(\theta) = \Sigma\, w_C(Cbrain_{model} - Cbrain_{exp})^2 + \Sigma\, w_M(Ma_{model} - Ma_{exp})^2 + \Sigma\, w_D(D_{model} - D_{hist})^2 + \lambda\|\theta - \theta_0\|^2 \quad (34)$$

was evaluated, with the weights w_C, w_M, and w_D specified in Subsection 2.4 and regularized toward the literature-based initial values θ_0, which preserves biological interpretability under the limited data.

Parameters fixed by the protocol—the LPS and GCS doses, the 2-h interval between GCS and LPS, the observation times and the physiological initial conditions—were not fitted. Fitting was restricted to coefficients with a clear biological interpretation that could be related to the calculated targets; $\beta_{brain} = 0.400$, $\eta = 0.600$, $\rho = 0.200$, $\kappa_{in} = 1.000$, and $k_{in} = 0.370$ were kept at their initial (regime A) values.

Three starting sets corresponding to the dynamic regimes A, B, and C were tested. $J(\theta)$ decreased from 18.42 to 0.97 (A), from 15.44 to 1.05 (B), and from 11.83 to 5.34 (C). The difference between A and B is too small to identify the realized regime, but regime C is supercritical in η ($2.863 > \eta_{crit} \approx 2.25$) and lies in the region where two attractors coexist, whereas the observed dynamics correspond to a resolving response with a delayed central component. The final parameter values, their confidence intervals, and their practical identifiability are given in Table 11.

Table 11. Final values of the model parameters after numerical calibration, their confidence intervals, and practical identifiability.

Parameter	Initial value (regime A)	After calibration	95% confidence interval	Change, %	Identifiability	Biological role
k_{BBB}	0.120	0.104	0.084–0.254	−13.1	Moderate (3.0-fold)	Transmission of the inflammatory signal across the BBB
δ_{brain}	3.000	0.799	0.400–1.035	−73.4	Moderate (2.6-fold)	Clearance of the central inflammatory response
κ_{out}	1.000	1.419	0.617–3.912	41.9	Low (6.3-fold)	Rate of microglial deactivation
K	1.164	0.147	0.121–0.205	−87.4	High (1.7-fold)	Threshold of microglial activation
k_{out}	1.224	2.409	1.160–3.772	96.8	Moderate (3.3-fold)	Rate of resolution of tissue damage
$IC_{50,C}$	0.800	0.616	0.153–1.485	−23.0	Low (9.7-fold)	Half-maximal GCS concentration, periphery
$IC_{50,N}$	0.800	0.469	0.363–0.943	−41.4	Moderate (2.6-fold)	Half-maximal GCS concentration, CNS
MP potency	0.900	1.028	0.973–1.360	14.2	High (1.4-fold)	Relative potency of methylprednisolone
β_{brain}	0.400	not fitted	-	-	-	Production of central mediators by activated microglia
η	0.600	not fitted	-	-	-	Sensitivity of microglia to central mediators
ρ	0.200	not fitted	-	-	-	Contribution of tissue damage to microglial activation
κ_{in}	1.000	not fitted	-	-	-	Rate of microglial activation
k_{in}	0.370	not fitted	-	-	-	Rate of tissue damage accumulation

Notes: The confidence intervals were obtained by parametric bootstrap (120 replicates): the group means were resampled from a normal distribution with the measured standard errors for five animals per group, after which the calibration procedure was repeated in full. The figure in parentheses in the identifiability column is the ratio of the upper bound of the interval to the lower one. Grades: high, up to 2-fold; moderate, from 2- to 5-fold; low, more than 5-fold. The parameters β_{brain}, η, ρ, κ_{in}, and k_{in} were not fitted: they enter the observables only through the ratios $\beta_{brain}/\delta_{brain}$ and k_{in}/k_{out}, which, with two observation time points, are absorbed by the observation scaling factors (Subsection 3.9).

The largest changes affected K (−87.4%), k_{out} (96.8%), and δ_{brain} (−73.4%); that is, the parameters that set the duration of the central response. $IC_{50,N}$ (0.469) is lower than $IC_{50,C}$ (0.616); within the model, the incomplete suppression of cerebral markers therefore arises from the structure of the system—local mediator production by microglia and the feedback loop through damage—and not from a weaker action of the drug in the CNS.

Model and experimental values were compared separately for C_{brain}, Ma, and D, since their ranges and measurement precision differ, with the inter-individual variability (±1 SEM across animals) shown for each point (Figure 6). Agreement was closest for the central inflammatory index (r = 0.860, CCC = 0.853, $\chi^2/df = 1.78$). For the microglial component, the correlation was comparable (r = 0.877, CCC = 0.869), but $\chi^2/df = 2.38$, the discrepancy arising mainly from the LPS group in the hippocampus, where the model underestimates activation. For the histological index, a high correlation (r = 0.834) was combined with a lower concordance (CCC = 0.656), reflecting a systematic offset with the correct ordering of groups preserved; agreement is formally not rejected ($\chi^2/df = 1.0$), and the largest fraction of points within ± 1 SEM (58.3%) follows from the wide variability of the semi-quantitative scores.

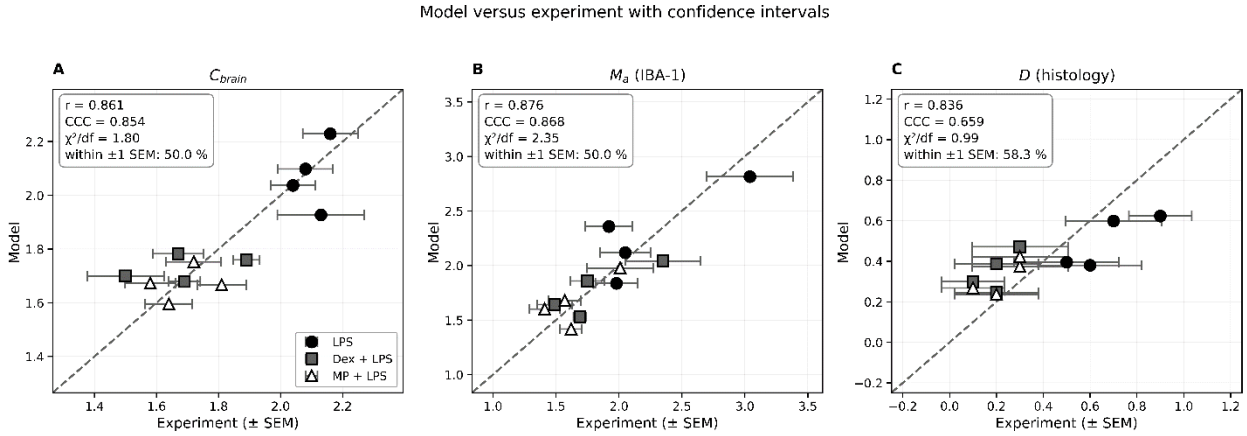

Figure 6. Experimental target values versus the corresponding model variables after numerical calibration (± 1 SEM across animals).

The model thus reproduces the principal experimental patterns: the rise of the central inflammatory response and of the microglial component after LPS, the presence of morphological damage, partial attenuation of the early changes under preventive GCS administration, and residual central changes by day 10. These metrics describe the goodness of fit on the same data used for calibration and are not an independent validation; with two time points and aggregated variables, the model should be regarded as a tool for interpreting the key patterns of neuroinflammation rather than for predicting absolute marker values.

3.10. Precision of the parameter estimates and practical identifiability

Parameter estimation was performed by nonlinear least squares using the trust-region reflective algorithm in a logarithmic parameterization, which guarantees positivity of the estimates, with a regularization term $\lambda\|\ln\theta - \ln\theta_0\|^2$ and $\lambda = 0.03$. The comparison was carried out at two time points (days 2 and 10) for two brain structures and three experimental groups, which gives 36 observations. The observation scaling factors s_C, s_M, and s_D were not included in the numerical search: the

observation equation is linear in them, so for each set of structural parameters, they were obtained explicitly by least squares.

Eight structural parameters were fitted: k_{BBB}, δ_{brain}, κ_{out}, K, k_{out}, $IC_{50,C}$, $IC_{50,N}$, and the relative potency coefficient of methylprednisolone. The remaining coefficients were fixed, since β_{brain}, κ_{in}, k_{in}, and ρ enter the observables only through the ratios $\beta_{brain}/\delta_{brain}$ and k_{in}/k_{out}, which, with two time points, are absorbed by the observation scaling factors; K_{BBB} is not separable from k_{BBB}; and α_C and α_N shifted by less than 3% in a preliminary run, indicating that the data are uninformative with respect to them.

The precision of the estimates was characterized in four ways: asymptotic Wald intervals, profile likelihood, parametric bootstrap (120 replicates), and posterior distributions obtained by ensemble sampling. The asymptotic intervals proved unusable, the relative standard errors ranging from 8% to 542%, which shows that the linear approximation does not apply in the neighborhood of the estimate; the other three methods gave consistent results, and the intervals they yield are those reported in Table 11.

The precision differs by an order of magnitude between parameters. Reliably determined are the microglial activation threshold K and the relative potency of methylprednisolone (interval widths below twofold); moderate precision is achieved for δ_{brain}, $IC_{50,N}$, k_{BBB}, and k_{out}; the least well determined are κ_{out} and $IC_{50,C}$, whose intervals span more than a sixfold range. The reasons differ: for κ_{out}, the likelihood profile reveals a competing branch corresponding to slow microglial deactivation, since with two observation time points, fast decay with high mediator production and slow decay with low production are indistinguishable; for $IC_{50,C}$, the peripheral variable C_{per} was not measured directly, so peripheral inhibition acts on the observables only indirectly. Biological interpretation is therefore admissible primarily for the first two groups, whereas κ_{out} and $IC_{50,C}$ are reported as working values. These results characterize the information content of the available data rather than a shortcoming of the model: improving them requires more observation time points and direct measurement of peripheral mediators, not a more complex model structure.

4. Study implications

4.1. Relationships among the model parameters

Equation (19) reduces the equilibrium problem of the eight-dimensional system to a single scalar condition in which the microglial sensitivity to central mediators, the rate at which activated microglia produce them, and the central clearance rate appear only as the ratio $\eta\,\beta_{brain}/\delta_{brain}$, compared with the activation threshold K. The parameters, therefore, act through the dimensionless central feedback gain $\Lambda = \eta\,\beta_{brain}/(\delta_{brain}\,K)$, the increase in the activation stimulus produced by one unit of microglial activation, expressed in units of the threshold. Several consequences follow.

First, the saddle-node transitions reported separately for η ($\eta_{crit} = 2.25$) and for β_{brain} ($\beta_{brain,crit} = 1.25$) are two sections of one critical surface $\Lambda = \Lambda_{crit}$: the corresponding products $\eta\cdot\beta_{brain}$ are 3.46 and 3.58, agreeing to within 4%, and both give $\Lambda_{crit} \approx 1.12$–$1.15$. Chronicity cannot, therefore, be attributed to any single parameter. It also follows that η, β_{brain}, δ_{brain}, and K are not separately identifiable from measurements confined to the central compartment; this is a structural limitation that no increase in the number of sampling times would remove, and it is why these coefficients had to be constrained by regularization in the calibration of Subsection 3.8.

Second, the central inhibitory function multiplies the whole activation stimulus, so that, under treatment, the effective gain is $\Lambda_{eff}(t) = I_N(X_e, R)\cdot\Lambda$. The glucocorticoid rescales the gain but does not displace the critical surface, and does so only transiently, as the drug is eliminated and R(t) accumulates. This is the structural explanation of the dissociation observed experimentally: the drug reduces the

drive that pushes the system toward the separatrix but cannot move the separatrix itself.

Third, because the drug is given as a single dose before the challenge, the trajectory is determined by $X_c(0) = X_{dose} \exp(-k_{el}\tau)$, so that dose and pre-treatment interval τ are exactly exchangeable within the model. This yields a falsifiable prediction: administering the same dose 4 h rather than 2 h before the stimulus should be equivalent to reducing the dose by about 14%, and an experiment in which interval and dose are varied jointly would test it.

Finally, no rate constant of the model corresponds to a long characteristic time—the slowest eigenvalue at the physiological equilibrium is $-0.700\ \text{day}^{-1}$, a relaxation time of approximately 1.4 days—so the persistence of central alterations at day 10 cannot reflect the slow clearance of any single mediator. It arises instead from capture by a second attractor once Λ exceeds Λ_{crit}, and is thus evidence of bistability.

4.2. Limitations of the approach

These limitations concern the method rather than the biology represented. The calibration was restricted and used the same material from which the model was built, so the agreement obtained is not validation; a formal analysis of structural identifiability was not performed, with practical identifiability being assessed as described in Subsection 3.9. The sensitivity analysis of Subsection 3.6 is local and of the one-factor-at-a-time type and, near the saddle-node, is valid only within the basin of attraction of the baseline solution, so the coefficients of Table 9 must not be extrapolated across the separatrix. The bifurcation analysis used two control parameters and sought saddle-node transitions only; the dependence of the separatrix on the pharmacological parameters, which governs how long a preventive dose protects the system, was not examined. The dose-dependent switching functions are phenomenological rather than mechanistic. The variable R(t) is a lumped surrogate that was not measured in the source experiment, and several distinct mechanisms would produce the same phenomenology. Finally, the description is deterministic and represents each group by a single average trajectory: in a bistable system, this is a substantive restriction, since a group mean may correspond to no individual trajectory at all, and the two glucocorticoids, sharing one pharmacokinetic structure, cannot be compared mechanistically.

4.3. Novelty of the study

The contributions of the present work are as follows. The peripheral and the central compartments are coupled through an explicit and variable blood–brain barrier flux, so that suppression of the peripheral response and persistence of the central one are separated within a single system instead of being represented by one aggregated mediator variable. The glucocorticoid enters not as a reduction of a cytokine term or as an abstract control variable but as a chain of measurable processes—pharmacokinetics, restricted transfer into brain tissue, two distinct inhibitory pathways, and a time-dependent decline in receptor-mediated efficacy—whose effect depends explicitly on the interval between administration and stimulus, which makes preventive dosing a property of the dynamics and yields the falsifiable dose–timing relation stated above. Most importantly, incomplete suppression of neuroinflammation and the persistence of central alterations at day 10 follow from a single structural fact rather than requiring two separate explanations: the drug rescales the feedback gain only transiently, whereas the position of the critical surface $\Lambda = \Lambda_{crit}$ is determined by parameters on which it does not act. A model in which the intervention is represented as a reduction of a cytokine term cannot generate this dissociation, because the drug and the feedback gain are not separated in it.

5. Conclusions

A model of neuroinflammation was constructed as a system of eight ordinary differential equations in which the peripheral and the central compartments are coupled by a saturable flux across the blood–brain barrier, and preventive treatment enters through the interval between dosing and the inflammatory stimulus rather than through the initial conditions alone. The system is well-posed: for non-negative initial data, the solution exists, is unique, and remains non-negative and bounded, and every equilibrium reduces to a single scalar condition for the activated microglial fraction, which permits a complete determination of the equilibria and of their local stability.

The course of neuroinflammation is governed not by the intensity of the external stimulus alone but by the gain of the central positive feedback circuit between inflammatory mediators and activated microglia. Three regimes were identified—rapid resolution, delayed recovery with persistent central alterations, and transition to a stable chronic state—with the first and the third being separated by a saddle-node bifurcation located at $\eta = 2.25$ and at $\beta_{brain} = 1.25$ for the two control parameters examined. Beyond this threshold, a chronic equilibrium coexists with the physiological one, and the unstable branch created together with it forms the boundary between their basins of attraction. The largest normalized sensitivities of the cumulative central inflammatory burden belong to the microglial activation threshold (−1.879) and to the central mediator clearance rate (−1.619).

The model therefore provides a mechanistic account of the experimentally documented failure of glucocorticoids to suppress neuroinflammation completely despite effective control of the peripheral response: the drug rescales the gain of the central circuit only transiently, as it is eliminated, and receptor-mediated efficacy declines, whereas the position of the critical threshold is determined by parameters on which it does not act. Persistence of central alterations at day 10 is accordingly reproduced not as the tail of a slow relaxation but as capture by a second attractor. Neuroinflammation is represented in aggregated form, without the cellular and regional heterogeneity of the central nervous system, the phenotypes of microglia and astrocytes, or the full spectrum of pro- and anti-inflammatory mediators; further development will introduce regional structure and additional cell populations, drug-specific pharmacokinetic profiles, and calibration against an independent dataset with a denser time grid.

Use of generative-AI tools declaration

During the preparation of this manuscript, the authors used the AI-based language editing tools Grammarly and Curie for grammar checking, language polishing, and improvement of clarity and readability. These tools were used only for editorial assistance and did not contribute to the generation of scientific ideas. All suggested changes were carefully reviewed and edited by the authors, who take full responsibility for the accuracy, originality, and integrity of the manuscript.

Conflict of interest

The authors declare no conflict of interest.

Author contributions

Elena Lebedeva: methodology, validation, investigation, writing-original draft. Ekaterina Kukushkina: conceptualization, methodology, writing-review and editing. Marina Karpenko:

conceptualization, supervision, writing-review and editing. All authors have read and approved the final version of the manuscript.

References

1. Müller L, Di Benedetto S (2025) Neuroimmune crosstalk in chronic neuroinflammation: microglial interactions and immune modulation. *Front Cell Neurosci* 19: 1575022. https://doi.org/10.3389/fncel.2025.1575022
2. Chen Y, Yin P, Chen Q, et al. (2026) Neurodegenerative diseases and immune system: from pathogenic mechanism to therapy. *Neural Regen Res* 21: 3387–3410. https://doi.org/10.4103/NRR.NRR-D-25-00274
3. Reichardt SD, Amouret A, Muzzi C, et al. (2021) The role of glucocorticoids in inflammatory diseases. *Cells* 10: 2921. https://doi.org/10.3390/cells10112921
4. Stahn C, Buttgereit F (2008) Genomic and nongenomic effects of glucocorticoids. *Nat Clin Pract Rheumatol* 4: 525–533. https://doi.org/10.1038/ncprheum0898
5. Samuel S, Nguyen T, Choi HA (2017) Pharmacologic characteristics of corticosteroids. *J Neurocrit Care* 10: 53–59. https://doi.org/10.18700/jnc.170035
6. Valotis A, Högger P (2007) Human receptor kinetics and lung tissue retention of the enhanced-affinity glucocorticoid fluticasone furoate. *Resp Res* 8: 54. https://doi.org/10.1186/1465-9921-8-54
7. Hochhaus G (2008) Relative receptor affinity comparisons among inhaled/intranasal corticosteroids: perspectives on clinical relevance. *Resp Res* 9: 75. https://doi.org/10.1186/1465-9921-9-75
8. Daley-Yates PT (2015) Inhaled corticosteroids: potency, dose equivalence and therapeutic index. *Br J Clin Pharmacol* 80: 372–380. https://doi.org/10.1111/bcp.12637
9. Buttgereit F, Brand MD, Burmester GR (1999) Equivalent doses and relative drug potencies for non-genomic glucocorticoid effects: a novel glucocorticoid hierarchy. *Biochem Pharmacol* 58: 363–368. https://doi.org/10.1016/S0006-2952(99)00090-8
10. Meijer OC, de Lange ECM, Breimer DD, et al. (1998) Penetration of dexamethasone into brain glucocorticoid targets is enhanced in mdr1A P-glycoprotein knockout mice. *Endocrinology* 139: 1789–1793. https://doi.org/10.1210/endo.139.4.5917
11. Karssen AM, Meijer OC, van der Sandt ICJ, et al. (2001) Multidrug resistance P-glycoprotein hampers the access of cortisol but not of corticosterone to mouse and human brain. *Endocrinology* 142: 2686–2694. https://doi.org/10.1210/endo.142.6.8213
12. Mason BL, Pariante CM, Thomas SA (2008) A revised role for P-glycoprotein in the brain distribution of dexamethasone, cortisol, and corticosterone in wild-type and ABCB1A/B-deficient mice. *Endocrinology* 149: 5244–5253. https://doi.org/10.1210/en.2008-0041
13. Sorrells SF, Sapolsky RM (2007) An inflammatory review of glucocorticoid actions in the CNS. *Brain Behav Immun* 21: 259–272. https://doi.org/10.1016/j.bbi.2006.11.006
14. Frank MG, Miguel ZD, Watkins LR, et al. (2010) Prior exposure to glucocorticoids sensitizes the neuroinflammatory and peripheral inflammatory responses to *E. coli* lipopolysaccharide. *Brain Behav Immun* 24: 19–30. https://doi.org/10.1016/j.bbi.2009.07.008
15. Frank MG, Watkins LR, Maier SF (2015) The permissive role of glucocorticoids in neuroinflammatory priming: mechanisms and insights. *Curr Opin Endocrinol Diabetes Obes* 22: 300–305. https://doi.org/10.1097/MED.0000000000000168

16. Foster-Powell A, Rostami-Hodjegan A, Meno-Tetang G, et al. (2025) Mathematical modeling of neuroinflammation in neurodegenerative diseases. *CPT Pharmacometrics Syst Pharmacol* 14: 1908–1922. https://doi.org/10.1002/psp4.70064
17. Han J, Zhang Z, Zhang P, et al. (2025) The roles of microglia and astrocytes in neuroinflammation of Alzheimer's disease. *Front Neurosci* 19: 1575453. https://doi.org/10.3389/fnins.2025.1575453
18. Vaughan LE, Ranganathan PR, Kumar RG, et al. (2018) A mathematical model of neuroinflammation in severe clinical traumatic brain injury. *J Neuroinflammation* 15: 345. https://doi.org/10.1186/s12974-018-1384-1
19. Batulin D, Lagzi F, Vezzani A, et al. (2022) A mathematical model of neuroimmune interactions in epileptogenesis for discovering treatment strategies. *iScience* 25: 104343. https://doi.org/10.1016/j.isci.2022.104343
20. Torres N, Molina E, Pujo-Menjouet L (2025) An optimal control problem for anti-inflammatory treatments of Alzheimer's disease. *J Math Biol* 91: 1. https://doi.org/10.1007/s00285-025-02227-8
21. Eftimie R, Gillard JJ, Cantrell DA (2016) Mathematical models for immunology: current state of the art and future research directions. *Bull Math Biol* 78: 2091–2134. https://doi.org/10.1007/s11538-016-0214-9
22. Chamberland É, Moravveji S, Doyon N, et al. (2024) A computational model of Alzheimer's disease at the nano, micro, and macroscales. *Front Neuroinform* 18: 1348113. https://doi.org/10.3389/fninf.2024.1348113
23. Lebedeva EYa, Kukushkina ES, Tyutunnik TV, et al. (2025) Glucocorticosteroid-induced behavioral changes during endotoxemia in rats. *Med Acad J* 25: 82–89. https://doi.org/10.17816/MAJ631323
24. Heneka MT, Carson MJ, Khoury JE, et al. (2015) Neuroinflammation in Alzheimer's disease. *Lancet Neurol* 14: 388–405. https://doi.org/10.1016/S1474-4422(15)70016-5
25. Hindmarsh AC (1983) ODEPACK, a systematized collection of ODE solvers, In: Stepleman, R.S., *Scientific Computing*, Amsterdam: North-Holland, 55–64.
26. Petzold L (1983) Automatic selection of methods for solving stiff and nonstiff systems of ordinary differential equations. *SIAM J Sci Stat Comput* 4: 136–148. https://doi.org/10.1137/0904010
27. Virtanen P, Gommers R, Oliphant TE, et al. (2020) SciPy 1.0: fundamental algorithms for scientific computing in Python. *Nat Methods* 17: 261–272. https://doi.org/10.1038/s41592-019-0686-2
28. Sheiner LB, Stanski DR, Vozeh S, et al. (1979) Simultaneous modeling of pharmacokinetics and pharmacodynamics: application to d-tubocurarine. *Clin Pharmacol Ther* 25: 358–371. https://doi.org/10.1002/cpt1979253358
29. Holford NHG, Sheiner LB (1982) Kinetics of pharmacologic response. *Pharmacol Ther* 16: 143–166. https://doi.org/10.1016/0163-7258(82)90051-1
30. Brent RP (1973) *Algorithms for Minimization without Derivatives*, Englewood Cliffs: Prentice-Hall.
31. Kuznetsov YA (2004) *Elements of Applied Bifurcation Theory*, 3 Eds., New York: Springer. https://doi.org/10.1007/978-1-4757-3978-7
32. Jolliffe IT (2002) *Principal Component Analysis*, 2 Eds., New York: Springer. https://doi.org/10.1007/b98835

33. Morris MD (1991) Factorial sampling plans for preliminary computational experiments. *Technometrics* 33: 161–174. https://doi.org/10.1080/00401706.1991.10484804
34. Marino S, Hogue IB, Ray CJ, et al. (2008) A methodology for performing global uncertainty and sensitivity analysis in systems biology. *J Theor Biol* 254: 178–196. https://doi.org/10.1016/j.jtbi.2008.04.011
35. Saltelli A, Annoni P, Azzini I, et al. (2010) Variance based sensitivity analysis of model output. Design and estimator for the total sensitivity index. *Comput Phys Commun* 181: 259–270. https://doi.org/10.1016/j.cpc.2009.09.018
36. Hartman P (2002) *Ordinary Differential Equations*, 2 Eds., Philadelphia: SIAM. https://doi.org/10.1137/1.9780898719222
37. Smith HL (1995) *Monotone Dynamical Systems: An Introduction to the Theory of Competitive and Cooperative Systems*, Providence: American Mathematical Society. https://doi.org/10.1090/surv/041
38. Hirsch MW, Smith HL (2006) Monotone dynamical systems, In: Cañada A, Drábek P, Fonda A, Author, *Handbook of Differential Equations: Ordinary Differential Equations*, Amsterdam: Elsevier, 239–357. https://doi.org/10.1016/S1874-5725(05)80006-9
39. Khalil HK (2002) *Nonlinear Systems*, 3 Eds., Upper Saddle River: Prentice Hall.
40. Hadamard J (1902) Sur les problèmes aux dérivées partielles et leur signification physique. *Princeton Univ Bull* 13: 49–52.

AIMS Press